國 立 交 通 大 學

電機與控制工程學系

碩士論文

以同步觀測圖和時相高階頻譜分析

來探討禪坐的心肺交互作用

Study on Meditation Cardiorespiratory Interactions

Based on Synchrogram and Time-phase Bispectral Analysis

研 究 生：蔡政恩

指導教授：羅佩禎 博士

中 華 民 國 九 十 六 年 十 月

以同步觀測圖和時相高階頻譜分析來探討禪坐的心肺交互作用

Study on Meditation Cardiorespiratory Interactions Based on Synchrogram and Time-phase Bispectral Analysis

研 究 生：蔡政恩　　Student：Jeng-En Tsai

指導教授：羅佩禎 博士　　Advisor：Dr. Pei-Chen Lo

國 立 交 通 大 學

電機與控制工程學系

碩 士 論 文

A Thesis

Submitted to Department of Electrical and Control Engineering

College of Electrical and Computer Engineering

National Chiao Tung University

In Partial Fulfillment of the Requirements

For the Degree of

Master

In

Electrical and Control Engineering

October 2007

Hsinchu, Taiwan, Republic of China

中 華 民 國 九 十 六 年 十 月

以同步觀測圖和時相高階頻譜分析來探討禪坐的心肺交互作用

研究生：蔡政恩　　指導教授:羅佩禎 博士

國立交通大學電機與控制工程學系

摘要

本研究的目的在於探討當心肺交互作用發生在禪坐時的相位同步和非線性交互作用。同步觀測圖和時相高階頻譜分析工具分別被用來研究相位同步和非線性交互作用。本研究共收集了 16 位年齡相似的受測者，其中實驗組為 7 位具有禪坐經驗者，而控制組 9 位受測者則無此經驗。由結果發現，發生同步的時段數、總維持時間和非線性交互作用的時段數都有顯著增加（p 值分別為 0.023, 0.034, 0.038）。根據此結果，禪坐時對於心肺同步現象的影響是很明顯地。關於探討同步和非線性交互作用結果的一致性，我們發現禪坐時的正相關顯著增加（p 值為 0.011），因此推測在發生非線性交互作用時，禪坐可能會增加心肺系統之間的同步現象。

Study on Meditation Cardiorespiratory Interactions Based on Synchrogram and Time-phase Bispectral Analysis

Student : Jeng-En Tsai **Advisor :Dr. Pei-Chen Lo**

Institute of Electrical and Control Engineering

National Chiao-Tung University

Abstract

The aim of this research was to investigate the phase synchronization and nonlinear coupling while cardiorespiratory interaction occurred during Zen meditation. Synchrogram analysis was applied to the investigation of phase synchronization, and time-phase bispectral analysis was employed in studying the nonlinear coupling. This study included 16 subjects, 7 experimental subjects with Zen-meditation experience and 9 control subjects in the same age range, yet, without any meditation experience. According to our results, number of the synchronous epochs, the total synchronization duration, and the number of the coupling epochs all significantly increased (p=0.023, 0.034, and 0.038, respectively) during meditation. As a result, the effect of meditation on cardiorespiratory synchronization was evident. Regarding the methodological coincidence between synchronization and nonlinear coupling, we found that positive correlation increased significantly (p = 0.011) during meditation. It suggests that under nonlinear coupling, meditation might enhance the phase synchronization between cardiac and respiratory systems.

誌　　謝

這篇論文的完成，首先要感謝指導教授羅佩禎老師的教導，不管在於研究上的科學邏輯思考、論文寫作的表達，還有生活處世上的態度，讓我獲益良多。同時也要感謝口試委員楊谷洋、陳永昇老師對於論文提出的許多指導和建議。

在碩士班的研究生涯中，我要特別感謝適達學長對於論文的方向、方法與寫作上的熱心指導。也感謝權毅、晏銘、憲正、政勳、進忠、偉凱學長、瑄詠學姊在這段時間給了我許多研究上的建議和鼓勵。還有謝謝一起努力的恩榮、博翔、宗仁、信丞、昶毅。另外，也感謝 buwonol 讓我學習講英文、嘉鴻為實驗室帶來的歡樂氣氛、家鈞在住宿上的幫忙、球友勁源和系桌的大家，讓我在研究之餘能夠放鬆身心。

最後我要感謝父母和家人們，謝謝你們的關心和支持，讓我能夠在沒有後顧之憂下完成學業。

Contents

List of Tables

List of Figures

Chapter 1
Introduction

1.1 Background and Motivation

The interaction between human cardiac and respiratory systems has been widely studied for many decades. It has been found that these two systems do not act independently; instead, they are coupled by some mechanisms. One well-known phenomenon of cardiorespiratory interaction is the frequency modulation of heart rate by respiration, which is known as respiratory sinus arrhythmia (RSA) [1]. RSA portrays the heart rate variability in synchrony with respiration, that is, the heart rate increases during inspiration and decreases during expiration. With RSA, human pulmonary air exchange can be more efficient [2]. In addition to modulation, other cardiorespiratory interaction such as synchronization has been observed, and the nature of interaction like nonlinear coupling was proposed in recent years [3-10].

Synchronization is a particular phenomenon that occurs due to interaction of two or more self-sustained oscillators [3]. This concept is widely used in various fields of science and engineering [11] and is interpreted in different ways when applied to different problems. In our study, we focused on the phase synchronization phenomenon in cardiorespiratory system. Details and definitions are described in Chapter 2.

In 1998, Schäfer et al. [4] applied the concept of phase synchronization of chaotic oscillators [12] to the development of a technique called ‘synchrogram’ to analyze irregular, non-stationary bivariate data. Based on this method, they found cardiorespiratory synchronization of several locking ratios (ratios of heartbeat

frequencies to respiratory frequencies) occurring in young healthy athletes at rest. This overthrew the widely accepted knowledge that cardiac and respiratory rhythms in humans were unsynchronized. Afterward several researches followed the synchrogram method and presented the phenomenon of cardiorespiratory phase synchronization on different subjects. Duration and frequency ratio are parameters of phase synchronization that have ever been investigated in these researches. Regarding the duration, long synchronous episodes were observed in young healthy athletes (about 1000 seconds) [3] and heart transplant patients (several hundreds of seconds) [5], while short episodes were observed in non-athlete normal subjects (less than 2 minutes) [6]. And there was no synchronous event detected in a critically ill patient in coma [7]. Bartsch et al. [8] showed that the occurrence of synchronization was significantly enhanced during non-rapid-eye-movement (non-REM) sleep (deep sleep and light sleep) and reduced during REM sleep. In the aspect of frequency ratio, a research on anaesthetized rats found that the frequency ratio upon phase synchronization would transit as the depth of anesthesia changed [9]. In spite of increasing researches devoted to this phenomenon in recent years, the mechanisms and meanings of cardiorespiratory phase synchronization are still not well understood. As a consequence, more researches are still needed to explore this emerging topic.

In addition to synchronization, the nature of coupling between cardiac and respiratory systems has been investigated. Bispectral analysis has been appealing to researchers during the last few years, particularly in investigating the presence of quadratic coupling in interacting harmonic oscillators [13]. For simplification, most studies consider biological systems to be stationary. In practical situations, however, interaction among subsystems often results in time-varying characteristics such as frequency and coupling strength. Hence, bispectral analysis based on time averaging for stationary signals is no longer sufficient. Time evolution of the bispectral

estimates is needed. In 2003, Jamšek et al. [14] proposed the time-phase bispectral analysis that introduced time dependence to the bispectral analysis of univariate data. In 2004, the method was used to detect the coupling phenomenon between cardiac and respiratory systems, and several episodes were detected (smaller than 2 minutes) [10].

As CAM (complementary and alternative medicine) becomes more popular in the West, scientific researches have been extensively carried out to justify the therapeutic effects of CAM and its benefits to human health. Among a large variety of approaches in CAM, meditation has been one of the most widely acceptable practices due to its substantial effectiveness and safety. It thus drew more attention from such professional areas as medicine, clinics, sciences, engineering, sociology, etc. According to numerous research reports since 1960's, meditation has been proved to benefit human health in various aspects. During meditation, the human body can be optimized by tuning up the brain-nervous system, cardiovascular system, respiratory system, etc. The phenomena and intrinsic mechanisms of such tune-up processes not only are of great interest but play an important role of exploring an optimal solution to human health maintenance.

For most meditation techniques, respiration is an important skill that ensures a good-quality meditation. Via specific respiration technique, human cardiovascular system may be influenced through cardiorespiratory interactions. There have been several researches aimed to investigate the cardiorespiratory interactions in different meditation schemes. In 1999, Peng et al. [15] observed very prominent low-frequency (~0.1Hz) oscillations in heart rate during specific forms of Chinese Chi and Kundalini yoga meditation in healthy young adults. In their later research [16], same phenomenon was also observed in two forms of meditations with different respiration techniques. In 2005, the RSA resulted from cardiorespiratory interactions was

investigated during Zen meditation. They concluded that low-frequency breathing could lead to in-phase RSA [17]. These researches showed that cardiorespiratory interactions during meditation were of unusual different features. However, except for RSA phenomenon, very few researches are performed to study the synchronization and nonlinear coupling of cardiorespiratory systems during meditation.

1.2 Aims of this Work

Our lab has been investigating the Zen-meditation EEG (electroencephalograph) since 1999. In recent years, we began studying the cardiovascular system-related physiological signals as well because they might be appropriate indicators for meditation effects on stress manipulation. This study was thus focused on ECG (electrocardiograph) and respiratory signals and aimed to investigate the phase synchronization and nonlinear coupling while cardiorespiratory interaction occurred during Zen meditation. Synchrogram was employed in the phase synchronization study, while time-phase bispectral analysis was used to quantify the nonlinear coupling. Moreover, we investigated the correlation between these two attributes.

1.3 Organization of this Thesis

This thesis is composed of five chapters. Chapter 1 describes the background, motivation, and main aim of this study. In Chapter 2, an introduction to ECG and respiratory signal is given, and the theories of synchrogram analysis and time-phase bispectral analysis are presented. In Chapter 3, the experimental setup and protocol are presented. Then the procedures for phase synchronization and nonlinear coupling analysis are illustrated. Chapter 4 reports and discusses the results. The last chapter makes a summary of this research and brings forward some issues for future study.

Chapter 2
Theories and Methods

Physiological signals play an important role in clinical diagnosis, and provide scientific indicators for the health of human body. Many physiological signals can be measured non-invasively and processed completely in digital form, for example, EEG (electroencephalograph), EMG (electromyograph), ECG (electrocardiograph), and respiratory signals. Since we mainly focused on the ECG and respiratory signals, Section 2.1 firstly gives a background introduction to these two signals. Section 2.2 describes the synchrogram method used to analyze the phase synchronization. Finally, to study the nonlinear coupling phenomenon, Section 2.3 presents the approach for time-phase bispectral analysis.

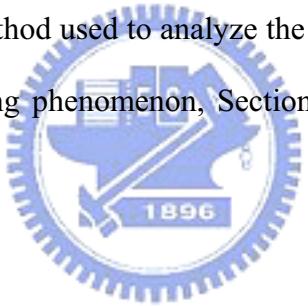

2.1 Introduction to ECG and Respiratory Signals

2.1.1 Introduction to ECG

Heart can beat by itself at a regular rhythm due to a specialized conducting system. The system comprises four parts, as shown in Fig. 2.1, SA node (sinoatrial node), AV node (atrioventricular node), Bundle of His, and Purkinje fibers. The SA node is the heart pacemaker that controls the beat rate of heart. Depolarization waves are generated by SA node and spread out to atria, AV node, and ventricles. When depolarization waves propagate to atria, atria contract resulting in emergence of “P” wave in ECG. These waves afterwards spread to AV node that connects with Bundle of His. Purkinje fibers are the extended parts of Bundle of His. The networking of

Purkinje fibers appears to be a threadlike net on subendocardial surface. Therefore, through Bundle of His, depolarization waves spread to entire ventricles and make two ventricles contract at the same time. In sum, the sequence of heart pumping is: SA node → atria → AV node → Bundle of His → Purkinje fibers → ventricles [18].

The depolarization waves not only spread throughout the whole heart, but also induce the electrical current change that can be non-invasively recorded on the body surface as the ECG signal. Without stimulation, the heart cells are in the quiescent state (approximate -80 mV) with negative potential (so-called polarization). Once being stimulated, they bear positive potential and the systole reaction is induced. Hence, ECG reflects the potential variation of rhythmic activity of the heart.

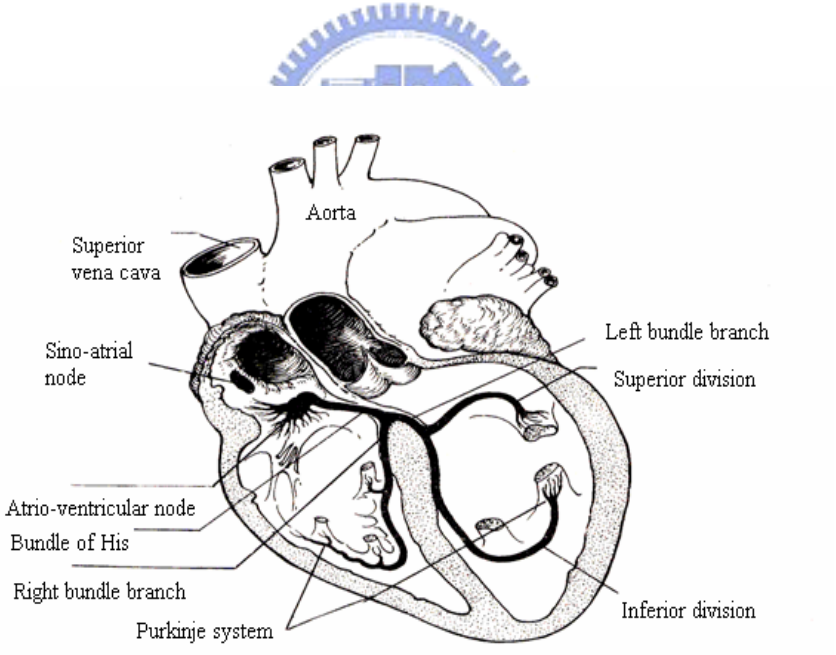

Fig. 2.1 The conducting system of heart [18].

The typical wave complex of ECG is shown in Fig. 2.2. The physiological meaning of each ECG complex pattern is described below:

P wave: The wave is due to the depolarization of atria. Atria contract at this time.

Q wave: The wave is caused by the depolarization of ventricles, and the R wave follows. Atria expand at this time.

R wave: The period of the depolarization of ventricles. Atria expand gradually, and ventricles start to contract at this time.

S wave: The period of the depolarization of ventricles. Atria completely expand, and ventricles completely contract.

T wave: This wave is due to the repolarization of ventricles. Ventricles expand gradually.

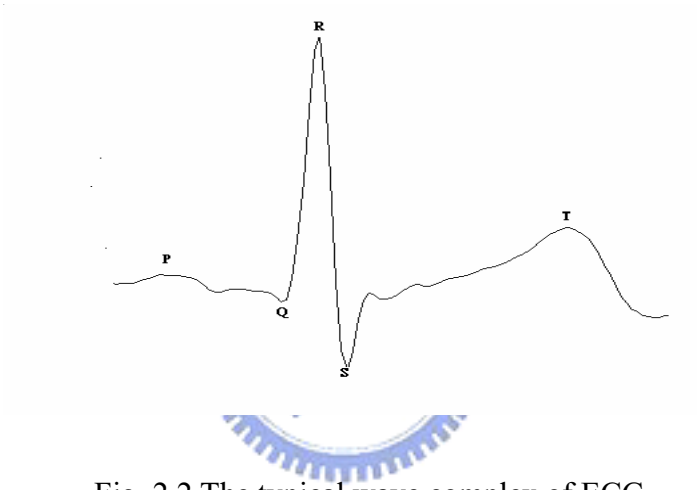

Fig. 2.2 The typical wave complex of ECG.

2.1.2 Introduction to Respiration

The respiration is responsible for bringing oxygen into the body and removing carbon dioxide out of the body. The mechanics of respiration involve muscles that change the volume of the thoracic cavity to generate inspiration and expiration. Two sets of muscles involved are the diaphragm and the intercostal muscles. The diaphragm is the wall separating the abdomen from the thoracic cavity that can move up and down. The intercostal muscles surround the thoracic cavity and are responsible for moving the rib cage in and out. As shown in Fig. 2.3, inspiration results from

contraction of the diaphragm (downward movement) and intercostal muscles (rib cage swings up and outward). Hence, the enlarged cavity housing the lungs has a pressure reduction of -3mm Hg with respect to the pressure outside the body, and the lung expands because of the difference of pressure. On the contrary, expiration results from the opposite mechanism. Using suitable instruments, the behavior of respiration can be recorded and transduced to an electrical signal [19].

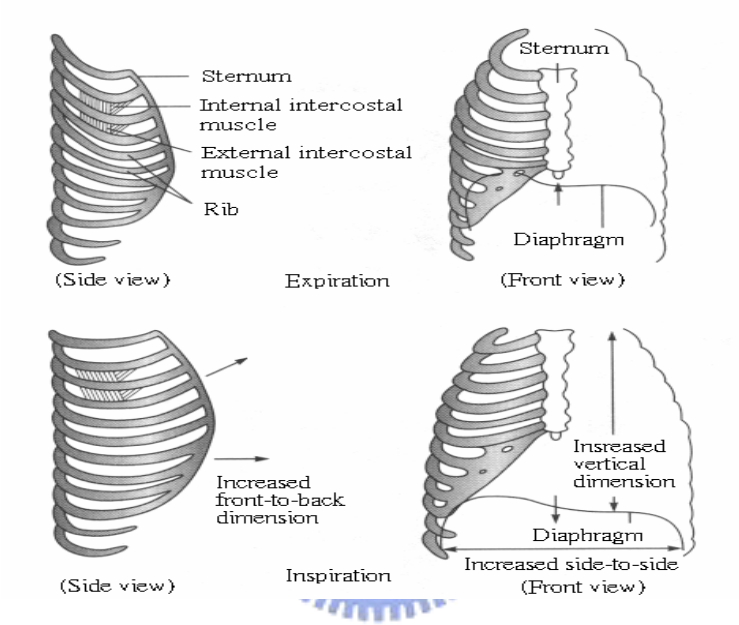

Fig. 2.3 Mechanics of expiration and inspiration [20].

2.2 The Synchrogram Method

2.2.1 Theory of Phase Synchronization

The phenomenon of synchronization is considered as an adjustment of rhythms, via specific manner of interaction, among distinctive self-sustained oscillators [3]. Such an interaction can lead to the locking of their phases, whereas their amplitudes may remain uncorrelated. Various definitions of *synchronization* have been proposed that require further description for each model-oriented, specific problem. In classical

sense of periodic self-sustained oscillators, synchronization is usually defined as locking (entrainment) of the phases,

$$\varphi_{n,m} = n\phi_1 - m\phi_2 = \text{const} \tag{2.1}$$

where n and m are integers, ϕ_1 and ϕ_2 are phases of two oscillators, and $\varphi_{n,m}$ is the generalized phase difference. Note that the values of ϕ_1 and ϕ_2 are not bounded in $[0, 2\pi]$. According to equation (2.1), oscillator 1 completes m cycles while oscillator 2 completes n cycles, and it is said to be a synchronization of m cycles of oscillator 1 with n cycles of oscillator 2. For generalization, a weaker condition for phase locking was proposed, as shown in equation (2.2) below, that can be feasible for nonlinear oscillators. In such cases, the n : m phase locking manifests as a variation δ of $\varphi_{n,m}$ around a horizontal plateau.

$$| \varphi_{n,m} - \text{const} | < \delta \tag{2.2}$$

In case of cardiorespiratory coupling, synchronization is usually influenced by the noise that originates not only from measurement and external disturbance but also from other subsystems taking part in the cardiovascular control [21]. Weak noise can lead $\varphi_{n,m}$ into fluctuation in a random way around a constant value, and strong noise may cause phase slips. As a consequence, the phenomenon of synchronization cannot be interpreted in a unique way, but be treated in a statistical sense. Follow the basic work of Stratonovich [22], phase locking in noisy systems is understood as the appearance of a peak in the distribution of the cyclic relative phase $\Psi_{n,m}$, and can be interpreted as the existence of a dominated stable value of phase difference between the two oscillators.

$$\Psi_{n,m} = \varphi_{n,m} \bmod 2\pi \tag{2.3}$$

where 'mod' is an operator converting the value of $\varphi_{n,m}$ into the range $[0, 2\pi]$ by

subtracting $2\pi k$ (k is an integer) such that $0 \le \Psi_{n,m} < 2\pi$.

2.2.2 Instantaneous Phase

Analysis of the synchronization between nonlinear oscillators requires quantification of the instantaneous phases of oscillators. In this thesis, we employed the method based on marker events to characterize the cyclic patterns of oscillators [23]. An example is illustrated in Fig. 2.4. The marker events are determined from the wave peaks. Then the instantaneous phase at any time t can be derived by the linear interpolation equation below,

$$\phi(t) = 2\pi \frac{t - t_k}{t_{k+1} - t_k} + 2\pi k \ , \ t_k \le t < t_{k+1} \tag{2.4}$$

where t_k is the time of the k^{th} marker event. The instantaneous phase of k^{th} marker event is $2\pi k$.

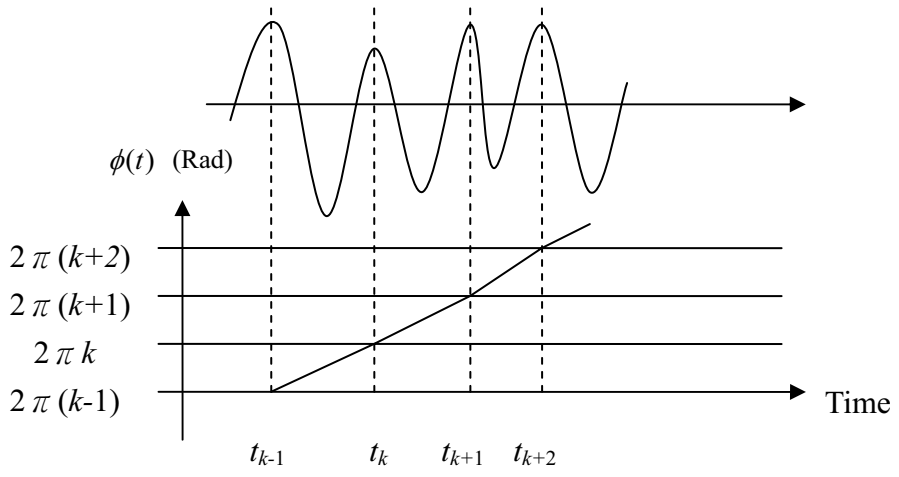

Fig. 2.4 Derivation of instantaneous phase using method based on marker events. In this example, the marker events are determined from the wave peaks.

2.2.3 Synchrogram Method and Quantification

The synchrogram method [3] was used to analyze the phase synchronization of two interacting self-oscillatory systems. The method is feasible for such cases like pseudo-periodic ECG with particular rhythmic events (R peak) occurring at given time instants. To plot the synchrogram, we need to determine the normalized relative phase $\psi_m(t_{k_2})$ of oscillator 1 at specific time instants that specific events of oscillator 2 occur. As described in equation (2.5), $\psi_m(t_{k_2})$ is obtained by wrapped phase ϕ_1 modulo $2\pi m$ (i.e., *m* consecutive cycles are viewed as one longer cycle), and is observed at time t_{k_2} when the marker events of oscillator 2 occur. Then the values of $\psi_m(t_{k_2})$ at time t_{k_2} are marked by dots along the vertical axis and the synchrogram is completed.

$$\psi_m(t_{k_2}) = \frac{1}{2\pi}[\phi_1(t_{k_2}) \bmod 2\pi m] \tag{2.5}$$

As an illustration, the synchrogram with $m = 2$ is shown in Fig. 2.5. It presents *n* dots within *m* consecutive cycles of oscillator 1.

In the ideal case of *n* : *m* synchronization, phase ϕ_1 within *m* cycles of oscillator 1 that grows from 0 to $2\pi m$ presents the same value at time t_{k_2} and t_{k_2+n}, i.e., $\psi_m(t_{k_2}) = \psi_m(t_{k_2+n})$. For example, $\psi_m(t_{k_2}) = \psi_m(t_{k_2+3})$ for the case of good synchronization illustrated in Fig. 2.6. In consequence, the synchrogram will manifest *n* horizontal lines. An advantage of this graphic tool is that only one integer of parameter *m* has to be chosen, and then several synchronous events with different integers of parameter *n* can be derived within one plot. Namely, various *n* : *m* synchronization conditions can be scrutinized based on a fixed valued of *m*, and the transitions between them can be traced.

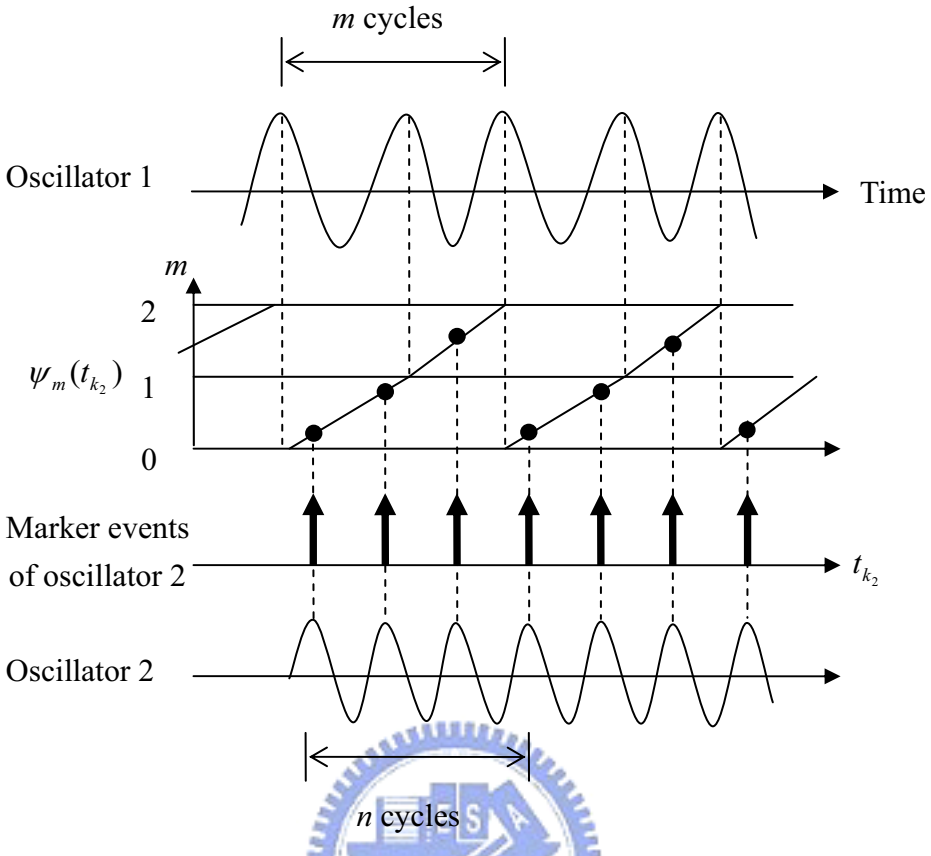

Fig. 2.5 Illustration of constructing the synchrogram.

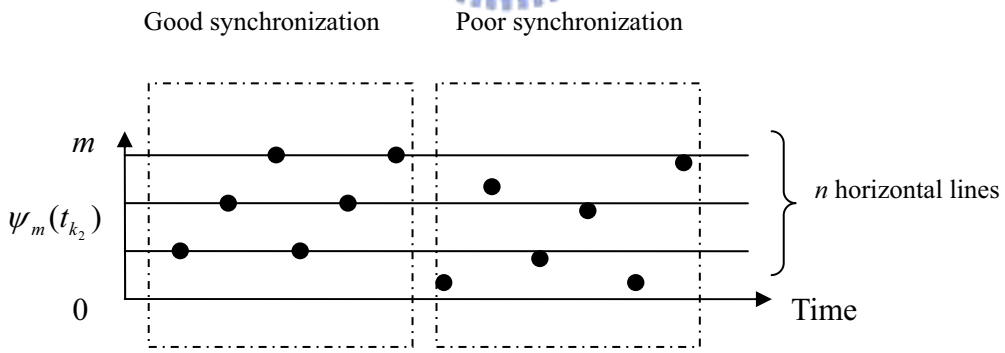

Fig. 2.6 Examples of good synchronization and poor synchronization.

Next, we develop the scheme for quantifying the synchronization phenomenon in addition to the graphical illustration by synchrogram. The examples of two different degrees of synchronization are presented in Fig. 2.6. High degree of n : m

synchronization (good synchronization) indicates that the values of $\psi_m(t_{k_2})$ are distributed regularly at the n specific values in the normalized range [0, m]. On the contrary, low degree of n : m synchronization (poor synchronization) is reflected by the random distribution of values of $\psi_m(t_{k_2})$.

Note that high degree of n : m synchronization introduces n horizontal lines within m adjacent cycles of oscillator 1. The scheme of quantification can be designed by examining how regular the distribution of values of $\psi_m(t_{k_2})$ is in the synchrogram. According to this concept, we first transform $\psi_m(t_{k_2})$ to $\Psi_{n,m}(t_{k_2})$ using equation (2.6). Then the degree $\gamma_{n,m}$ of n : m synchronization can be evaluated by equation (2.7) [24].

$$\Psi_{n,m}(t_{k_2}) = \frac{2\pi}{m}\left\{[\psi_m(t_{k_2}) \cdot n] \bmod m\right\} \tag{2.6}$$

$$\gamma_{n,m} = \{\frac{1}{N}\sum_{k_2}\cos[\Psi_{n,m}(t_{k_2})]\}^2 + \{\frac{1}{N}\sum_{k_2}\sin[\Psi_{n,m}(t_{k_2})]\}^2 \tag{2.7}$$

where N represents the number of marker events of oscillator 2 in a given window length. The value of $\gamma_{n,m}$ ranges from 0 to 1, where $\gamma_{n,m} = 1$ indicates the case of complete synchronization, and $\gamma_{n,m} = 0$ reveals the fact of complete desynchronization.

An example of complete n : m synchronization is shown in Fig. 2.7. The synchrogram illustrates n horizontal lines within the normalized range [0, m], with equidistance d between adjacent lines. The bottom line begins with $\psi_m(t_{k_2}) = d_1$. By equation (2.6), n horizontal lines are mapped to a constant value $\Psi_{n,m}(t_{k_2}) = 2\pi d_1 / d$, and $0 \le \Psi_{n,m}(t_{k_2}) < 2\pi$. According to equation (2.7), degree of synchronization is

$\gamma_{n,m} = 1$, reflecting the occurrence of complete synchronization.

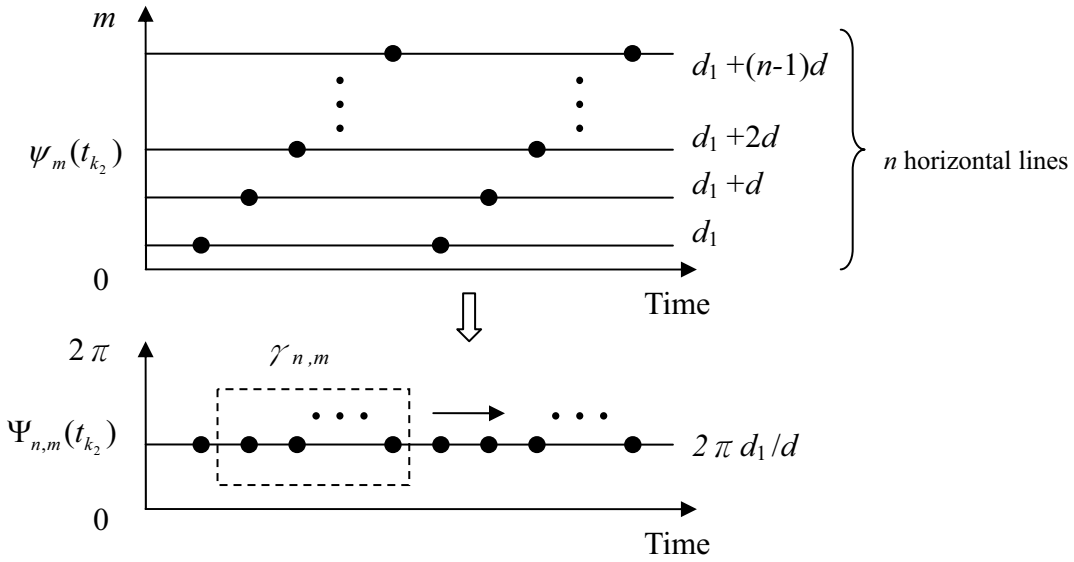

Fig. 2.7 The process of quantifying the degree of synchronization: an example of complete n : m synchronization.

2.3 Time-phase Bispectral Analysis

2.3.1 Classical Bispectral Analysis

Bispectral analysis belongs to a group of techniques based on high-order statistics (HOS) that can be used to analyze non-Gaussian signals, to obtain phase information, to suppress Gaussian noise of unknown spectral form, and to detect and characterize signal nonlinearities [13]. Besides, bispectral analysis is also a tool to observe the property of nonlinear (quadratic) phase coupling between oscillators.

The bispectrum involves third-order statistics. Its spectral estimation mainly adopts the direct, conventional Fourier transformation applied to the third-order moments. In the case of third-order statistics, the third-order moments are equivalent to third-order cumulants. From the above, classical way of estimating the bispectrum

$\hat{B}(k,l)$ is to evaluate the average of estimated third-order moments $\hat{M}_3^i(k,l)$,

$$\hat{B}(k,l) = \frac{1}{K}\sum_{i=1}^{K}\hat{M}_3^i(k,l) \tag{2.8}$$

where $\hat{M}_3^i(k,l)$ is the triple product of discrete Fourier transforms (DFTs) at discrete frequencies k, l, and $k + l$,

$$\hat{M}_3^i(k,l) = X_i(k)X_i(l)X_i^*(k+l), \qquad i = 1,...,k \tag{2.9}$$

where $X_i(.)$ is the discrete Fourier transform of signal $x[n]$. The signal is divided into K segments to obtain the statistical stability of the estimates.

Bispectrum $\hat{B}(k,l)$ is a complex function, characterized by its magnitude function A and phase function ϕ, also known as biamplitude and biphase, respectively.

$$\hat{B}(k,l) = |\hat{B}(k,l)|\, e^{j\angle\hat{B}(k,l)} = A(k,l)\, e^{j\,\phi(k,l)} \tag{2.10}$$

Bispectrum $\hat{B}(k,l)$ quantifies the quadratic coupling between two underlying oscillatory components of a signal. That is, the relation among the oscillations at two basic frequencies k and l, and a harmonic component at the frequency $k + l$ is examined. The set of three frequencies is known as a triplet (k, l, $k + l$). Strong coupling implies that the oscillatory components at k and l may have a common generator, and such components may synthesize a new component at the combinatorial frequency $k + l$ if a quadratic nonlinearity is presented.

To observe the coupling information between two signals $x[n]$ and $y[n]$, the cross bispectrum $B_{xyx}(k,l)$ is adopt. The coupling information among X at frequency k, Y at frequency l, and X at frequency $k + l$ can be examined. As shown below, cross bispectrum is estimated by

$$\hat{B}_{xyx}(k,l) = \frac{1}{K}\sum_{i=1}^{K} X_i(k)Y_i(l)X_i^*(k+l) \tag{2.11}$$

2.3.2 Time-phase Bispectral Analysis

The classical bispectral analysis is appropriate for studying stationary signals. In practical systems, interactions among subsystems often result in time variability of their characteristic frequencies. Accordingly, time-phase bispectral analysis that encompasses time dependence within the bispectral analysis was proposed [14].

In analogy with the short-time Fourier transform, the *M*-point DFT of signal $x(n)$ at time m is calculated by employing a moving window $w(n-m)$,

$$X(k, m) = \frac{1}{M}\sum_{n=0}^{M-1} x(n)\, w(n - m)\, e^{-j2\pi nk/M} \tag{2.12}$$

where k is the discrete frequency and n is the discrete time. Following equations (2.8), (2.9), and (2.11) while substituting $\{X(k,m), Y(l,m), X^*(k+l,m)\}$ for $\{X(k), Y(l), X^*(k+l)\}$ and letting $i=1$, the time-phase cross-bispectral analysis of signal x and y is

$$\hat{B}_{xyx}(k, l, m) = X(k, m)Y(l, m)X^*(k+l, m) \tag{2.13}$$

Similar to equation (2.10), the biamplitude and biphase functions can be obtained by the following equations.

$$\hat{B}_{xyx}(k,l,m) = |\hat{B}_{xyx}(k,l,m)|\, e^{j\angle\hat{B}_{xyx}(k,l,m)} = A_{xyx}(k,l,m)\, e^{j\,\phi_{xyx}(k,l,m)} \tag{2.14}$$

$$\phi_{xyx}(k,l,m) = \phi_x(k,m) + \phi_y(l,m) - \phi_x(k+l,m) \tag{2.15}$$

When two frequency components k and l of, respectively, X and Y signals are coupled, the last term in (2.15) becomes $\phi_x(k+l,m) = \phi_x(k,m) + \phi_y(l,m)$, resulting

in the biphase value of either 0 or 2π radian. Because dependent frequency components in a system may have phase difference, phase-coupling estimation requires less strict conditions and is able to reflect the existence of phase coupling in a wider sense. In addition, biamplitude function can be used to infer the relative strength of interaction between spectral components. As a consequence, the degree of coupling is determined by the magnitude of biamplitude and the observation of constant biphase. The degree of constant biphase γ_ϕ (a constant) can be quantified by equation (2.16) below [24].

$$\gamma_\phi = \{\frac{1}{N}\sum_m \cos[\phi_{xyx}(k,l,m)]\}^2 + \{\frac{1}{N}\sum_m \sin[\phi_{xyx}(k,l,m)]\}^2 \qquad (2.16)$$

where *N* represents the number of points in a given window length, and γ_ϕ is a value between 0 and 1. Biphase degree $\gamma_\phi = 1$ indicates a complete constant biphase, and $\gamma_\phi = 0$ is referred to the case of completely random biphase behavior.

Chapter 3
Experiment and Signal Analysis

In this chapter, the setup and procedure of experiments are first introduced. Next, implementation strategies and parameters are presented, particularly for applying the synchrogram analysis and time-phase bispectral analysis to ECG and respiratory signals

3.1 Experimental Setup and Procedure

This study involved two groups of subjects, the experimental group including subjects with Zen-meditation experience and the control group including subjects without any meditation experience. Background of subjects in each group is listed in Table 3.1.

Table 3.1 Subjects of experimental and control groups

	Experimental group	Control group
Number of subjects	7	9
Sex (male : female)	5 : 2	8 : 1
Age (years)	26.4 ± 2.5	25.3 ± 3.3
Meditation experience (years)	5.9 ± 2.6	

The experimental procedure of this study is illustrated in Fig. 3.1. Because the human cardiac function can be regulated by autonomic nervous system (ANS), the

experiments were conducted during the same period (3:00pm to 5:00pm) to ensure the approximately same state of ANS of all subjects. The experiments comprised two sessions. During Session 1, subjects of both groups rested, in a ~70° head-up back-tilt position with eyes closed, for 10 minutes. During Session 2, subjects of control group continued resting for 20 minutes; on the other hand, experimental subjects began meditation for 20 minutes. Experimental subjects, following their routine meditation habit, meditated with either full-lotus or half-lotus posture, with eyes closed. During meditation, practitioners concentrated their mind on "Zen Chakra" that was an energy point inside the third ventricle of human brain. All subjects breathed spontaneously in both sessions.

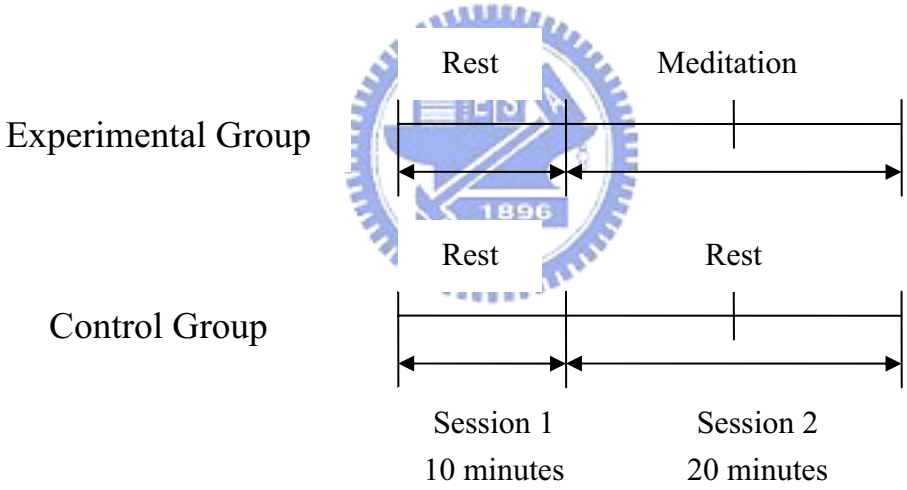

Fig. 3.1 Experimental procedure.

As shown in Fig. 3.2, ECG and respiratory signals were measured using PowerLab biosignal recording system (ADInstruments, Sydney, Australia) and then displayed and saved on a personal computer using the software Chart4 (ADInstruments, Bella Vista, Australia).

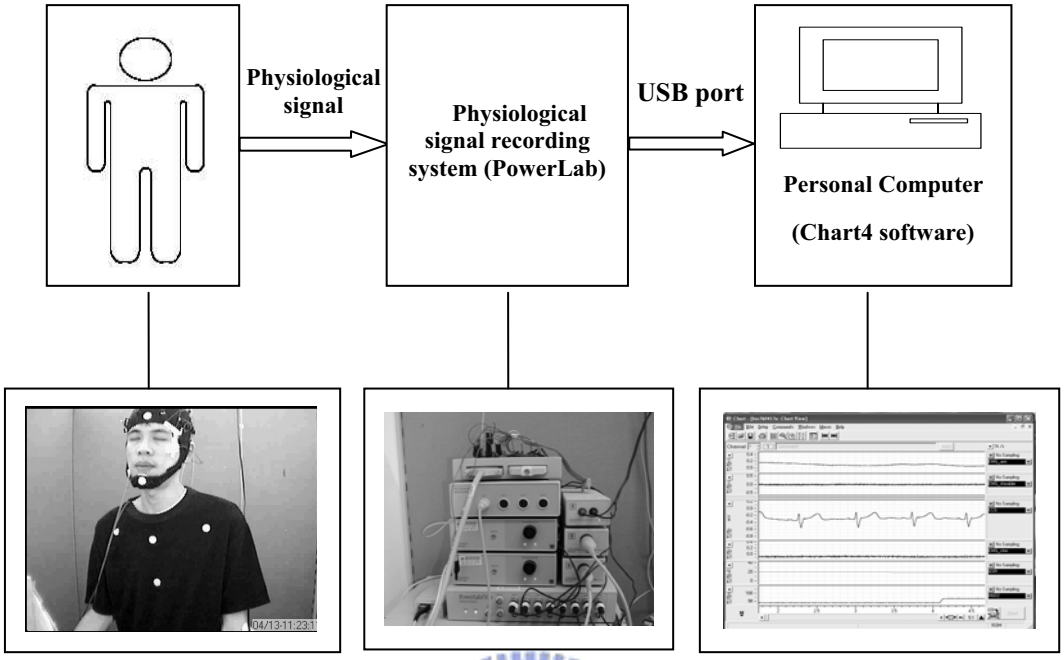

Fig. 3.2 The physiological signal recording system.

3.1.1 Measurement of ECG signal

The ECG signal was recorded using Lead I of standard bipolar limb leads [25], as shown in Fig. 3.3 (a). Electrode site on the left (right) arm was connected to the amplifier's positive (negative) input, with the ground on the inside of left ankle. The disposable ECG electrodes (Medi-Trace 200 Foam Electrodes, Kendall, Chicopee, MA, USA) as shown in Fig. 3.3 (b) were applied in this study. The ECG was pre-filtered by a 0.3-200 Hz bandpass filter and digitized by a sampling rate of 1000 Hz.

(a) (b)

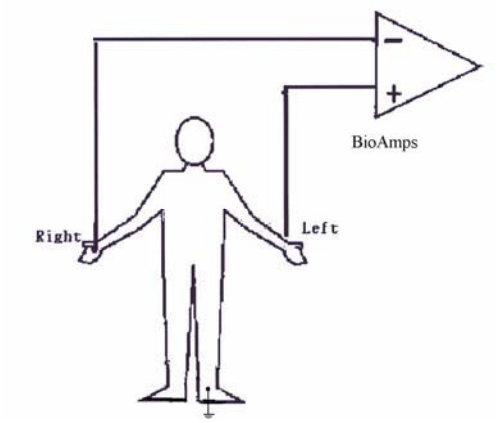

Fig. 3.3 (a) Lead Ⅰ configuration of bipolar limb leads, (b) Disposable ECG electrode.

3.1.2 Measurement of Respiratory Signal

Respiratory signal was recorded using a piezo-electric transducer (Model 1132 Pneumotrace II (R), UFI, Morro Bay, CA, USA) as shown in Fig. 3.4, that was wrapped around the belly passing the navel. The respiratory signal was pre-filtered by a lowpass filter with cutoff frequency of 5 Hz and digitized at the sampling rate of 1000 Hz. An example of respiratory signal is shown in Fig. 3.5. Note that the amplitude increases during inspiration and decreases during expiration.

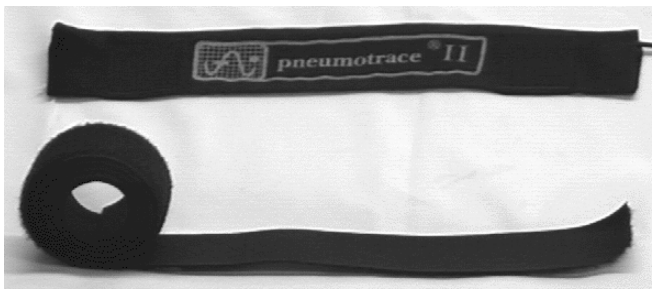

Fig. 3.4 Piezo-electric respiratory transducer.

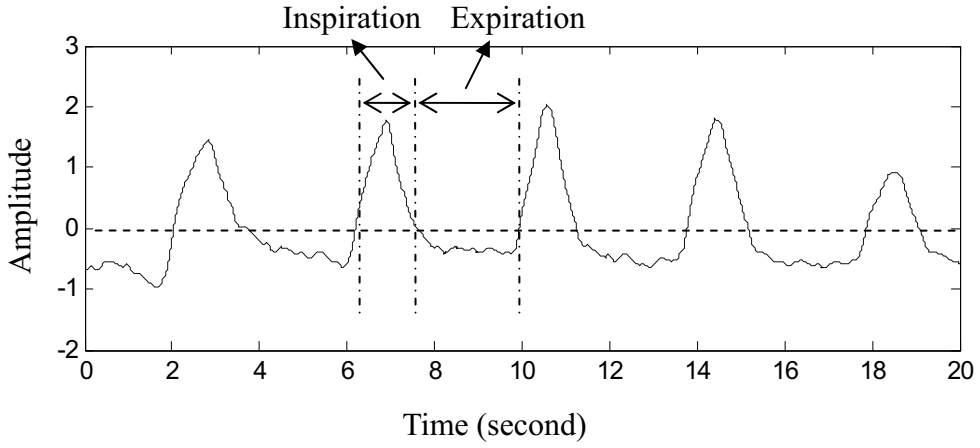

Fig. 3.5 Respiratory signal.

3.2 Strategies for Synchronization Analysis

The flow chart of synchronization analysis is shown in Fig. 3.6. The pre-processing stage was aimed to detect the R peaks of ECG and all the inspiration-phase peaks of respiratory signal. Then the instantaneous phases and frequencies were derived so that the synchrogram was ready to be constructed. At last, the synchronization length was quantified to evaluate the degree of synchronization for further comparison and interpretation.

Step 1. Pre-processing

Power spectrums of QRS complexes and respiratory signals are approximately 10-30 Hz and 0.2-0.3 Hz [21, 26, 27]. Accordingly, in pre-processing stage, we applied Matlab's built-in polyphase filter implementation, including anti-aliasing (lowpass) FIR filter, to down-sample the raw ECG and respiratory signals, respectively, to the rate of 200 samples and 20 samples per second. Then the algorithms described in Appendix A were applied to the detection of R peaks of ECG and inspiration-phase peaks of respiratory signal.

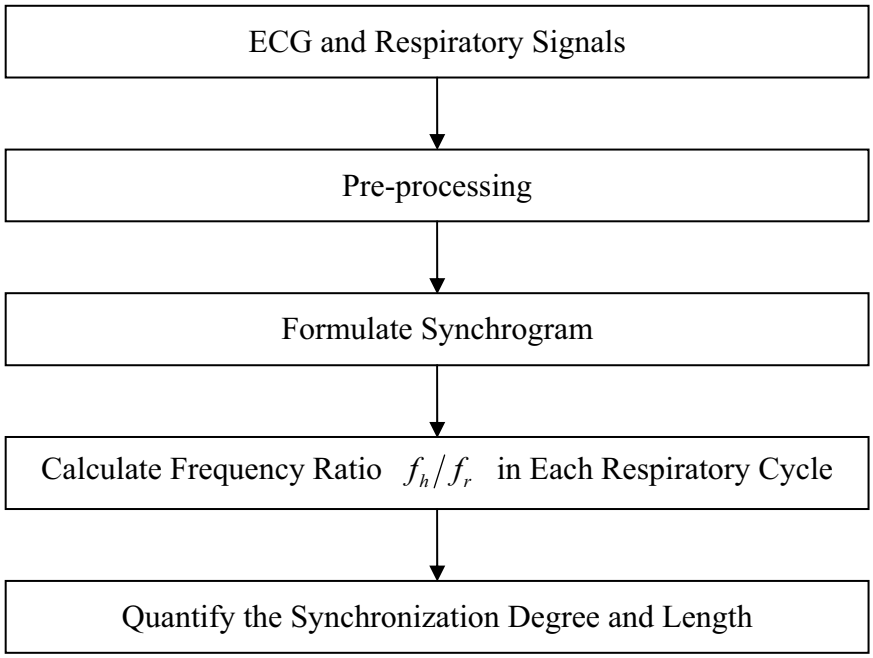

Fig. 3.6 Flow chart of synchronization analysis.

Step 2. Formulate Synchrogram

After peak detection, time positions of respiratory peaks were extracted as the marker events. Note that two adjacent marker events are considered as one complete cycle and a phase increase of 2π was assumed. Then, following equations (2.4)-(2.5), the normalized relative phase of respiratory signal could be determined.

To construct the cardiorespiratory synchrogram, we sketched the normalized relative phase $\psi_m(t_{k_2})$ of respiratory signal at time t_{k_2} identified as the appearances of R peaks of ECG. In this research, we observed the cardiorespiratory synchronization within 3 respiratory cycles. Therefore, only three synchrograms need to be plotted for each subject, i.e. n : 1, n : 2, and n : 3 synchrograms.

As an example, Fig. 3.7 displays three synchrograms derived for an experimental subject during meditation. Apparently, synchronization is evidently observed within

the range of 12-18 minutes, according to the piecewise, nearly parallel behaviors of n's curves in synchrograms.

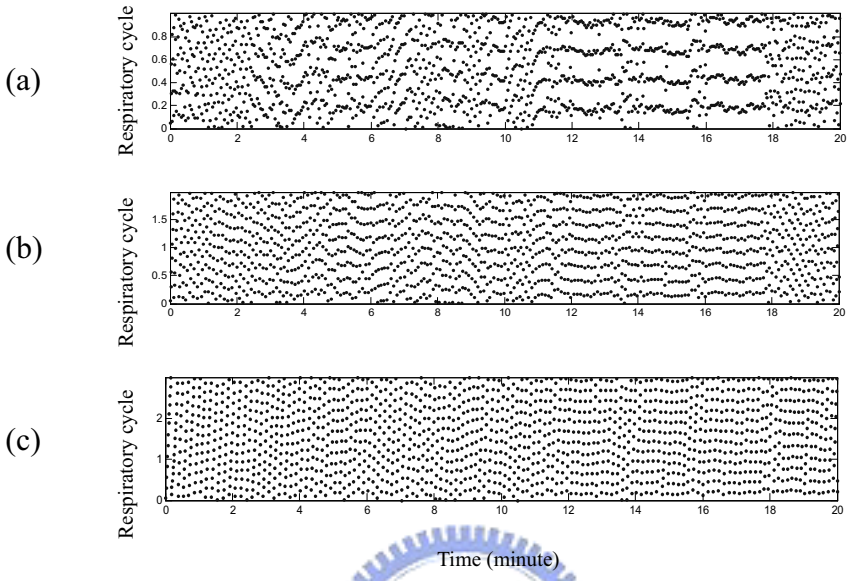

Fig. 3.7 The synchrograms of an experimental subject during meditation: (a) n : 1 synchrogram (b) n : 2 synchrogram (c) n : 3 synchrogram.

Step 3. Calculate Frequency Ratio f_h/f_r in Each Respiratory Cycle

The instantaneous frequency of heart beating f_h was calculated by inversing the time interval between two adjacent R peaks of ECG signal, while that of the respiration f_r was the reciprocal of the time interval between two respiratory peaks. Each computed value was placed in the mid point of two adjacent peaks (see Fig. 3.8 (b) and (d)). To calculate instantaneous frequency ratio f_h/f_r within each respiratory cycle, the instantaneous frequency of heart beating at the mid point of two adjacent respiratory peaks was estimated by linear interpolation (refer to Fig. 3.8 (e)).

As an illustrating example, Fig. 3.9 displays the sequence of instantaneous frequency ratio f_h/f_r of an experimental subject during meditation.

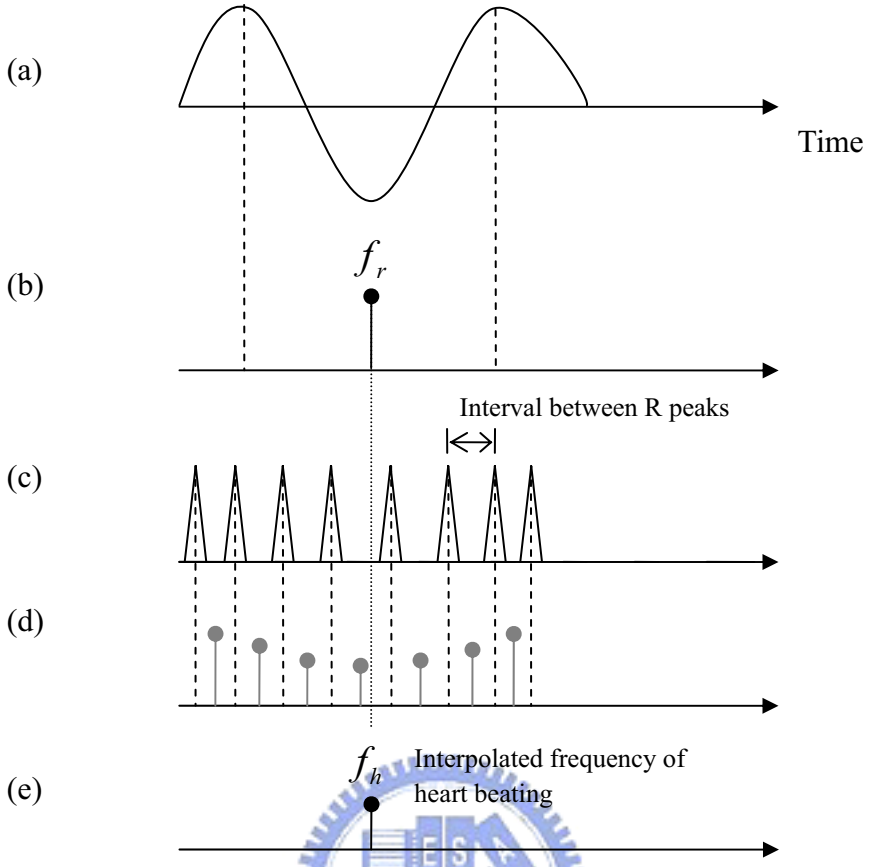

Fig. 3.8 Instantaneous frequency of heart beating and respiration: (a) Respiratory signal, (b) f_r: instantaneous frequency of respiration, (c) ECG signal, (d) Instantaneous frequency of heart beating, (e) f_h: instantaneous frequency of heart beating within a respiratory cycle.

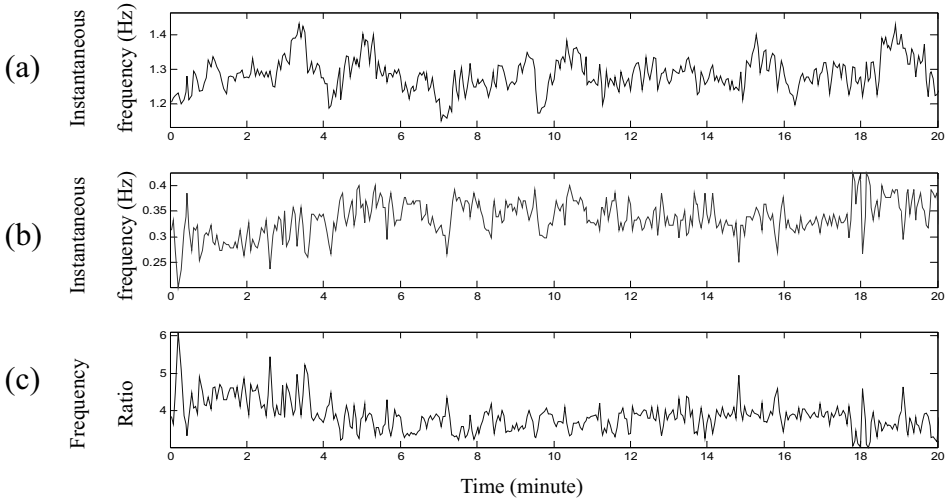

Fig. 3.9 (a) Time-varying sequence of f_h, (b) time-varying sequence of f_r, and (c) the sequence of frequency ratio f_h / f_r of an experimental subject during meditation.

Step 4. Quantify the Synchronization Degree

To evaluate the synchronization degree, the following procedure was proposed:

(1) The maximum and minimum values of frequency ratio, $min[f_h/f_r]$ and $max[f_h/f_r]$, were derived.

(2) According to the maximum and minimum ratio, we determined all possible pairs of (n,m)'s such that n/m satisfied: $min[f_h/f_r] \le n/m \le max[f_h/f_r]$. Note that all pairs (n/m)'s, after being reduced, were considered to be the same if they resulted in the same ratio. For example, only pair (4,1) was kept for the ratios of 4:1 and 8:2.

(3) Following equations (2.6)-(2.7), synchronization degree, $\gamma_{n,m}(t_{k_2})$, of qualified (n,m) pairs could be calculated with a window centered at time t_{k_2}. In this study, we employed the window length of 60 consecutive R peaks, with the moving step size of one R peak.

As an illustration, Fig. 3.10 demonstrates the time-varying synchronization degrees for all possible (n,m) pairs for an experimental subject during meditation. Based on this figure, significant synchronization is observed for the frequency ratio of 4:1, 7:2, and 11:3, respectively, in the time interval 12-18, 6-7, and 18-20 minute.

(4) The synchronization degree at a given time $t_{k_2}=T_{sd}$ was determined by finding the maximum value along the vertical line defined by $\gamma_{n,m}(t_{k_2}=T_{sd})$. The result was denoted by $\gamma_{\max}(t_{k_2}=T_{sd})$.

As an example, the sequence $\gamma_{\max}(t_{k_2})$ of an experimental subject during meditation is shown in Fig. 3.11.

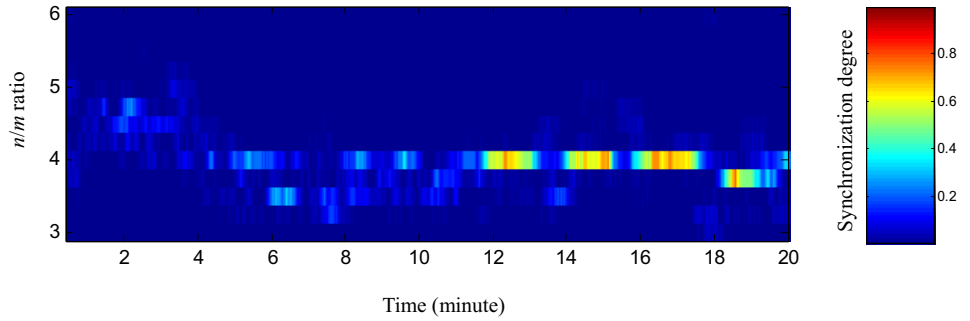

Fig. 3.10 Synchronization degrees for all possible (*n,m*) pairs for an experimental subject during meditation. The right color bar denotes the scale mapping for color representation.

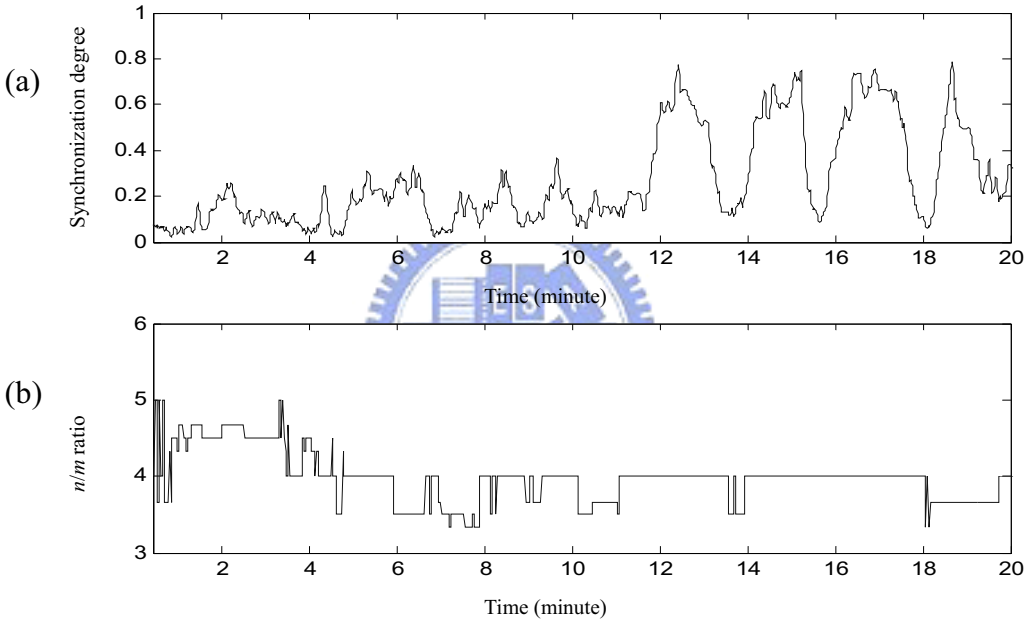

Fig. 3.11 (a) Time-varying synchronization degree, $\gamma_{\max}(t_{k_2})$, and (b) corresponding *n*/*m* ratio that the maximum synchronization degree was detected at the given time t_{k_2} (subject: a meditator during meditation).

Step 5. Quantify the Synchronization Duration

To evaluate the effective duration of synchronization, we first determined a threshold of synchronization degree, α. As shown in Fig. 3.12, synchronization duration measured the total duration in time with the degree of synchronization no

less than α.

To systematically determine the value of α, the following procedure was proposed:

(1) The values of $\gamma_{\max}(t_{k_2})$ were averaged every minute and the mean values were denoted as $\gamma_{\text{mean}}(t)$.

(2) The histograms of $\gamma_{\text{mean}}(t)$ were illustrated in Fig. 3.13 for both the experimental group (Fig. 3.13 (a)) and control group (Fig. 3.13 (b)).

(3) We found that the largest value of the histogram occurred at $\gamma_{\text{mean}}(t)$=0.2. Therefore, the threshold was determined to be α = 0.2.

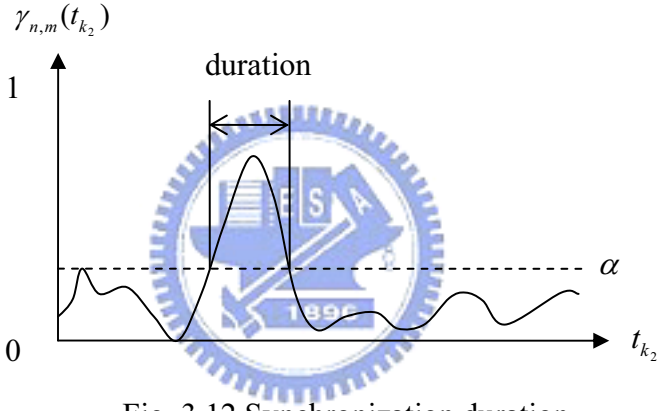

Fig. 3.12 Synchronization duration.

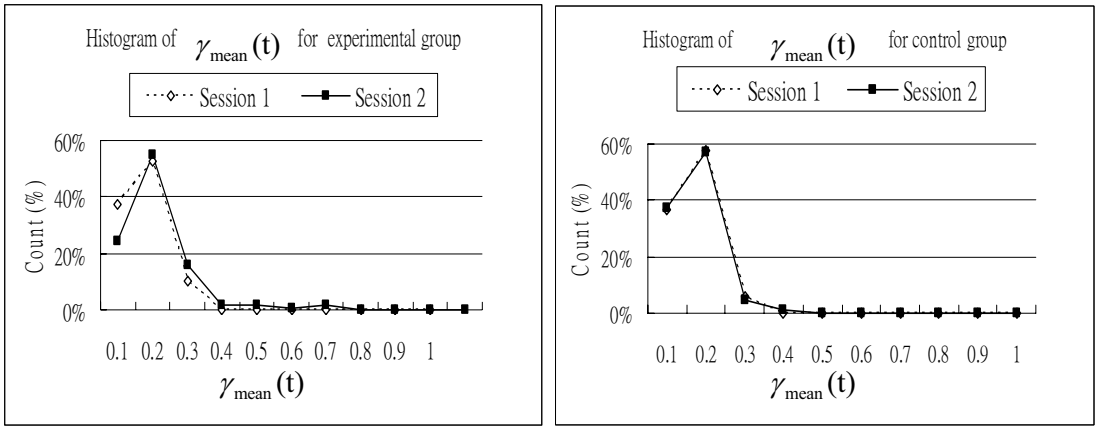

(a) (b)

Fig. 3.13 Histogram of $\gamma_{\text{mean}}(t)$ for (a) experimental group, and (b) control group.

3.3 Strategies for Time-phase Bispectral Analysis

Time-phase bispectral analysis was proposed to investigate the phenomena of phase coupling between ECG and respiratory signals. The flow chart of time-phase bispectral analysis is shown in Fig. 3.14.

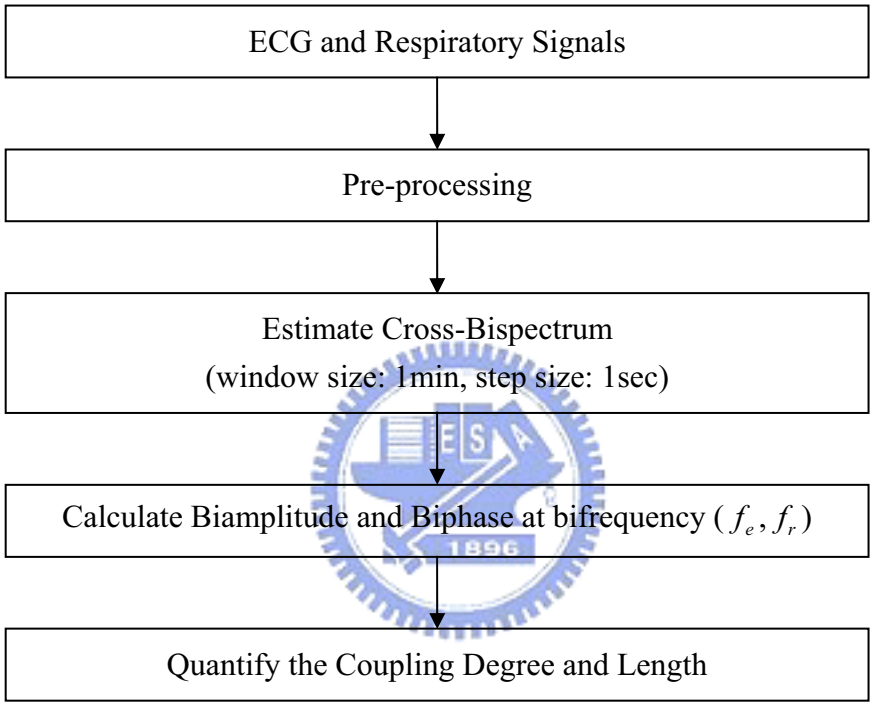

Fig. 3.14 Flow chart of time-phase bispectral analysis.

Step 1. Pre-processing

Fundamental frequencies of ECG and respiratory signals are approximately 1.2 Hz and 0.3 Hz [21]. Accordingly, raw ECG and respiratory signals originally recorded with sampling rate of 1000 Hz were downsampled to 10 Hz using Matlab's built-in polyphase filter implementation, including anti-aliasing, lowpass FIR filter with cutoff frequency 5 Hz. Then Chebyshev I IIR highpass filter with cutoff frequency 0.04 Hz was used to remove the baseline drift.

Step 2. Estimate Cross-Bispectrum

By equation (2.13), the cross-bispectrum $\hat{B}_{xyx}(k,l,m)$ was estimated. Here, k represents the frequency of ECG signal, l represents the frequency of respiratory signal, and m represents the time. The length of time window was selected to be 10 times of the period of slower signal, i.e. respiratory signal, to get reliable FFT (fast Fourier Transform) result. The slowest frequency of respiratory signals in our study was about 0.2 Hz (period: 5 sec per breath). We thus selected the window length to be 1 minute. To observe the time-varying behavior in more details, the moving step was selected to be 1 second.

Step 3. Calculate Biamplitude and Biphase at Bifrequency (f_e, f_r)

Using equation (2.14), biamplitude and biphase were evaluated at bifrequency (f_e, f_r) for each window frame. The bifrequency (f_e, f_r) of each window was determined by the maximum-power frequencies of ECG and respiratory signals respectively. Fig. 3.15 displays the example of one-minute cross-bispectrum for an experimental subject during meditation.

Step 4. Quantify the Coupling Degree

The coupling degree is determined by

$$\lambda(m) = A_{normalized}(m) \times \gamma_{\phi}(m) \tag{3.1}$$

where $A_{normalized}(m)$ is the normalized biamplitude for a given window, that is derived by first dividing the biamplitude by total power of cross-bispectrum in $0 \le f_e, f_r \le f_s/2$ and then normalizing the results of all subjects to the range [0 1]. The $\gamma_{\phi}(m)$, denoting the constant degree of biphase, can be calculated by equation (2.16) for a given window centered at time *m*. Fig. 3.16 illustrates the analyzing procedure for investigating the coupling degree of an experimental subject during meditation.

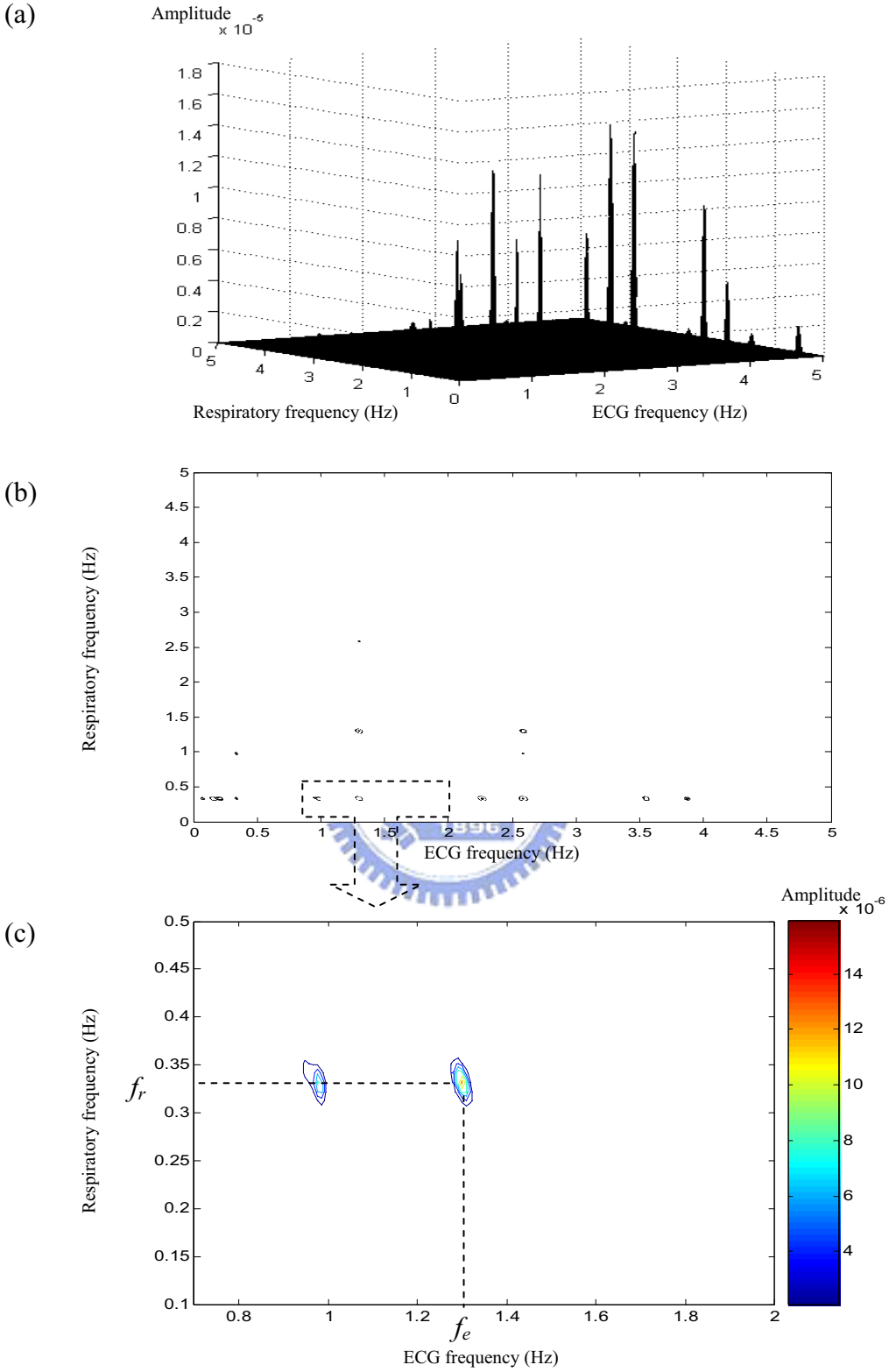

Fig. 3.15 (a) One-minute cross-bispectrum for an experimental subject during meditation, (b) its contour illustration, and (c) the zoom-in of contour illustration.

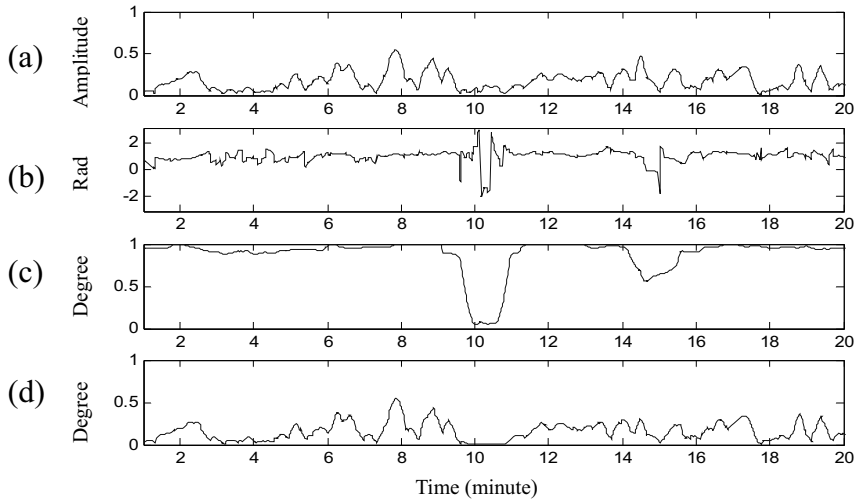

Fig. 3.16 The curves of (a) normalized biamplitude, $A_{normalized}(m)$, (b) biphase, $\phi(m)$, (c) constant degree of biphase, $\gamma_{\phi}(m)$, and (d) coupling degree, $\lambda(m)$, of an experimental subject during meditation.

Step 5. Quantify the Coupling Length

Coupling length provides an index of characterizing the duration of significance of phase coupling during the entire process. To quantify the coupling length, a threshold α needs to be determined first. To determine an appropriate value of α, the following procedure was proposed:

(1) A new sequence $\lambda_{\text{mean}}(t)$ containing the results of moving average of $\lambda(m)$ was obtained using a window size of one minute without overlap.

(2) The histogram of $\lambda_{\text{mean}}(t)$ was derived. Fig. 3.17 illustrates the histograms for experimental group (Fig. 3.17 (a)) and control group (Fig. 3.17 (b)).

(3) Maximum of the histogram (here, 0.2) indicates the majority of phase-coupling distribution. Accordingly, we selected α = 0.2 for this specific case.

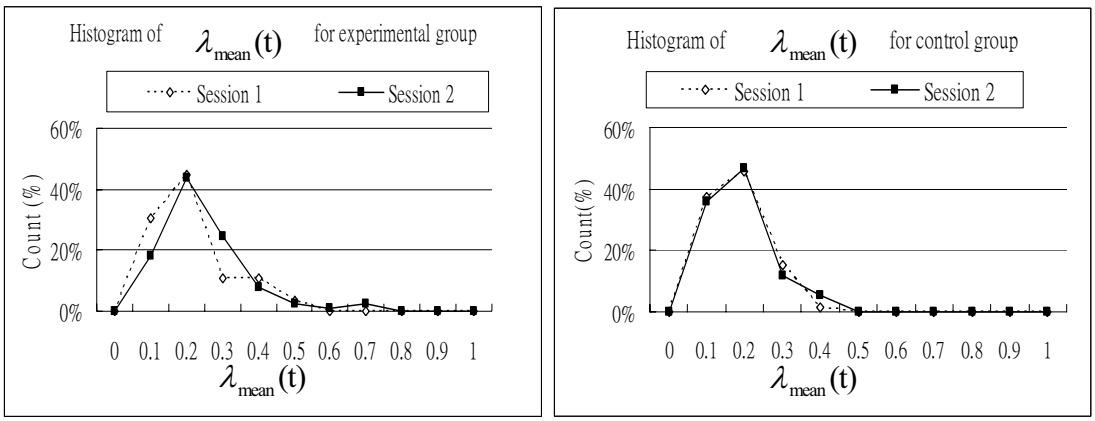

(a) (b)

Fig. 3.17 The histogram of $\lambda_{mean}(t)$ for (a) experimental group and (b) control group.

Chapter 4
Results

This chapter presents the results of synchronization analysis and time-phase cross-bispectral analysis. In addition, correlation between the synchronization and the nonlinear coupling was examined based on these results.

4.1 Results of Synchronization Analysis

To investigate the effects of meditation on cardiorespiratory synchronization, we compared three parameters, that is, lasting length, number of epochs, and total length, between the experimental and control group. The paired *t* test was applied to examine the significant difference of parameters between Session 1 and Session 2. The results are summarized in Table 4.1 and further explained in the following sub-sections.

Table 4.1 Mean values of three synchronization parameters analyzed for the experimental and control group.

	Experimental Group (n=7)		Control Group (n=9)		*p*-Value for comparison of	
	S1	S2	S1	S2	Exp. Group S1 vs. S2	Con. Group S1 vs. S2
Lasting length (seconds/epoch)	27.9±19.6	21.4±15.3	17.3±7.6	24.9±15.7	0.226	0.161
Number of epochs (counts/10 minutes)	2.3±1.5	4.0±2.4	2.6±1.5	2.3±1.9	0.023*	0.355
Total length (seconds/10 minutes)	55.6±34.9	107.0±92.4	51.8±35.0	47.5±34.2	0.034*	0.360

S1= Session 1; S2=Session 2; Exp.=Experimental group; Con.=Control group; *Significantly different ($p<0.05$).

4.1.1 Comparison of Lasting Length

The definition of "lasting length" here is the duration (refer to Fig. 3.12) of an epoch with synchronization degree higher than threshold. The histograms of lasting length of synchronization are presented in Fig. 4.1 for both groups. It shows that most synchronization epochs emerged from 10 to 30 seconds for both groups. And there is no apparent difference between groups and between sessions of each group on this distribution. That is, neither inter-group nor intra-group difference was observed. By statistical analysis for the mean values of lasting length of synchronization, both groups revealed no significant difference between two sessions, as shown in Fig. 4.2 and Table 4.1. This indicates that, in general, neither meditation nor rest could noticeably affect the lasting length of synchronization.

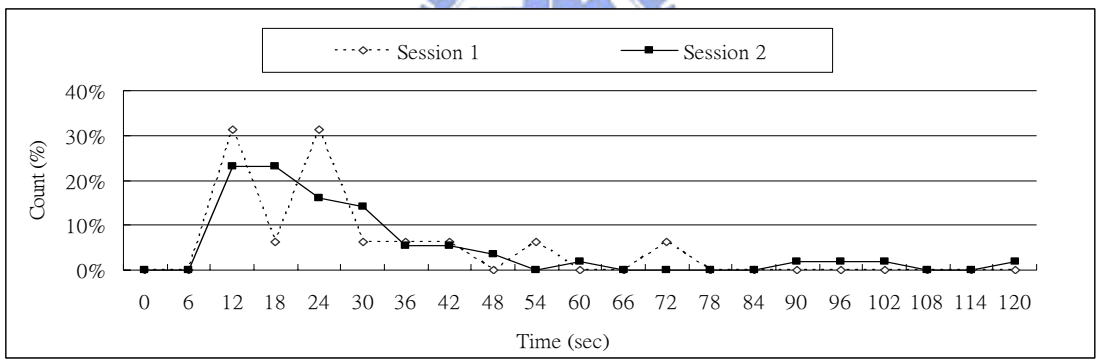

(a)

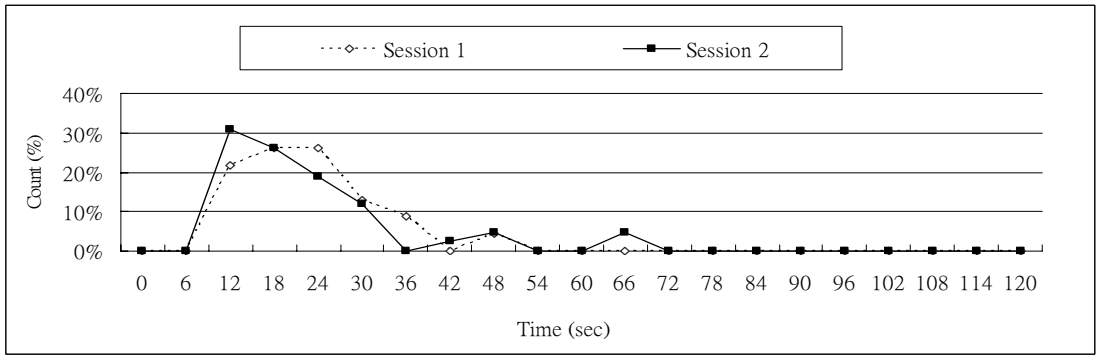

(b)

Fig. 4.1 Histograms of lasting length of synchronization for (a) experimental group, and (b) control group.

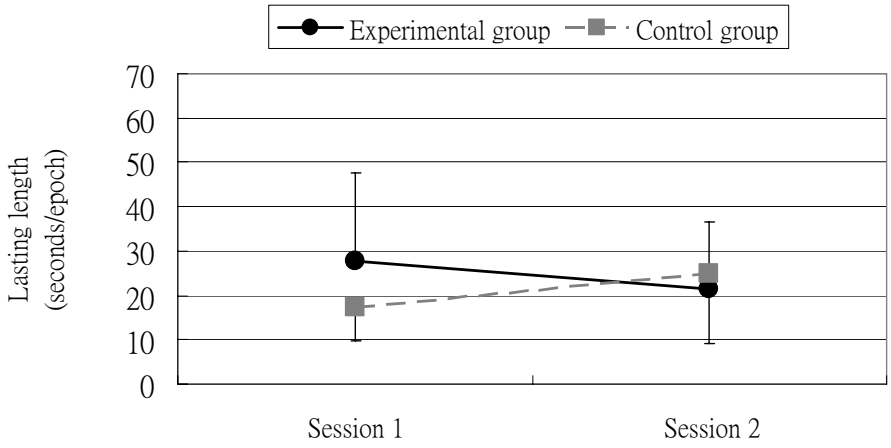

Fig. 4.2 Mean values of lasting length of synchronization for both groups in different recording sessions.

4.1.2 Comparison of Number of Epochs

The definition of "number of epochs" here is the amount of epochs with synchronization degree higher than threshold in a ten minutes time duration. As shown in Fig. 4.3 and Table 4.1, mean values of the number of synchronization epochs revealed insignificant difference between main session (Session 2, at rest) and pre-session (Session 1, background recording) in control group. As regards the experimental group, it increased considerably during meditation (Session 2: 4.0±2.4 counts/10 minutes), in comparison with the mean number observed in the pre-session background recording (2.3±1.5 counts/10 minutes).

4.1.3 Comparison of Total Length

The definition of "total length" here is the sum of lengths of all epochs with synchronization degree higher than threshold in a 10 minutes time period. According to the analysis in 4.1.2, we may anticipate similar results for comparing the total length of synchronization. As shown in Fig. 4.4 and Table 4.1, mean values of the total length of synchronization indeed did not change from pre-session to main-session recording in control group. However, experimental group exhibited an

almost twice increase in the total length of synchronization during meditation (Session 2: 107.0±92.4 seconds/10 minutes) while compared with the background recording in Session 1 (55.6±34.9 seconds/10 minutes).

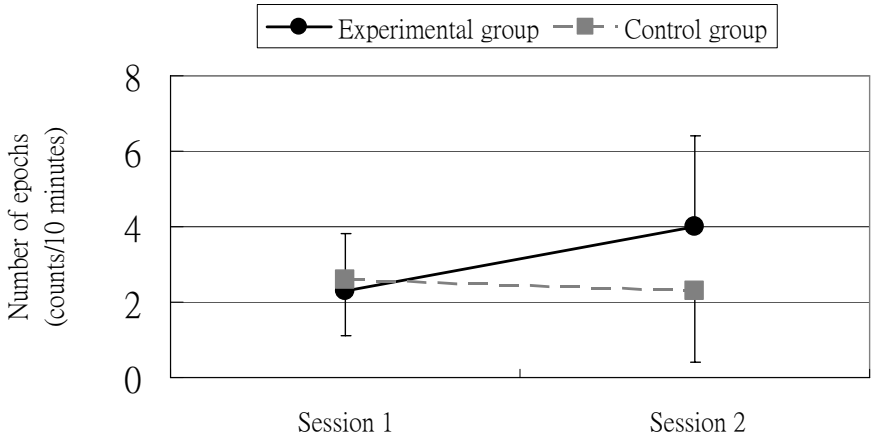

Fig. 4.3 Variations of mean number of synchronization epochs for both groups in different recording sessions.

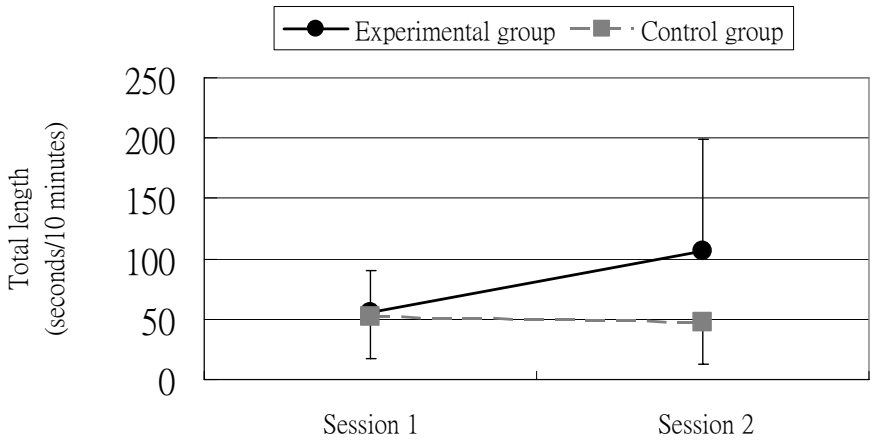

Fig. 4.4 Mean values of the total synchronization length for both groups in different recording sessions.

Further, we investigated the synchronization length for various (n/m) ratios. Fig. 4.5 displays the average length of synchronization (in seconds) versus (n/m) ratio. According to Fig. 4.5 (a), significant increase in the length of synchronization was

observed in experimental group at the ratio (n/m) = 4 (i.e., 4:1 synchronization) in the main-session recording, from which we may infer that one respiration accompanied four heart beats during the Zen-meditation course. On the other hand, the control group only revealed a slight increase at the ratio (n/m)=4.7 (i.e., 14:3 synchronization) in the (pre-session) background recording, without any particular event in the main-session recording (refer to Fig. 4.5 (b)).

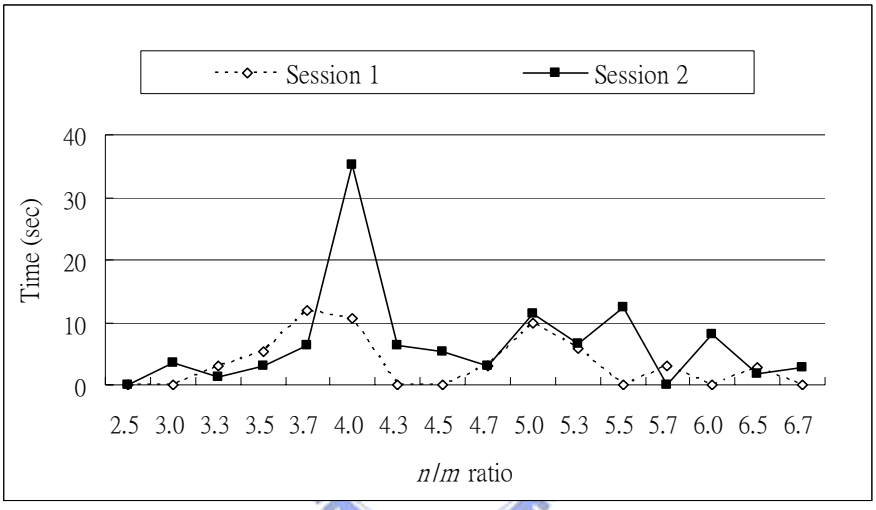

(a)

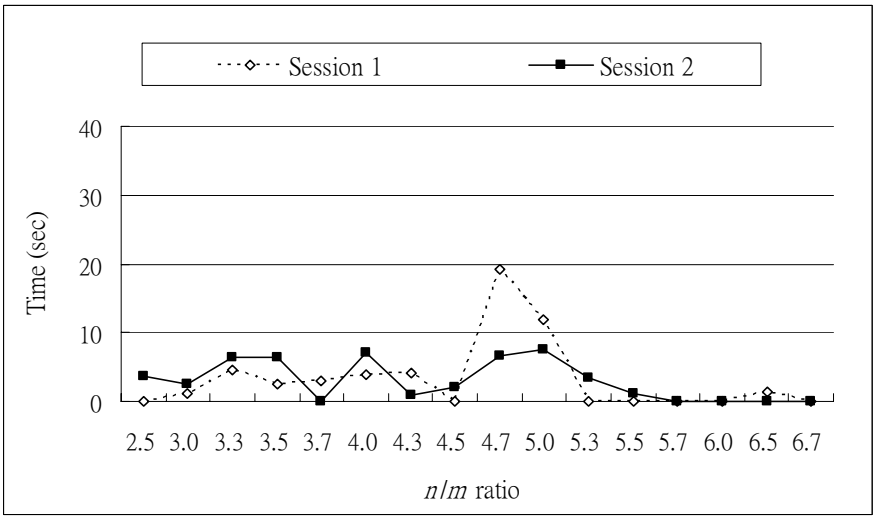

(b)

Fig. 4.5 Average length of synchronization for different (n/m) ratios in (a) experimental group and (b) control group.

4.2 Results of Time-phase Bispectral Analysis

To investigate the effects of meditation on cardiorespiratory coupling, we compared three parameters, that is, lasting length, number of epochs, and total length, are compared between experimental group and control group. The paired *t* test was applied to examine the significant difference of parameters between Session 1 and Session 2. The results are summarized in Table 4.2 and further explained in the following sub-sections.

Table 4.2 Mean values of three nonlinear coupling parameters analyzed for the experimental and control group.

	Experimental Group (n=7)		Control Group (n=9)		*p*-Value for comparison of	
	S1	S2	S1	S2	Exp. Group S1 vs. S2	Con. Group S1 vs. S2
Lasting length (seconds/epoch)	30.6±12.7	32.8±16.6	20.1±13.4	24.5±12.9	0.399	0.221
Number of epochs (counts/10 minutes)	4.1±2.3	6.1±2.5	3.6±3.3	4.0±2.7	0.038*	0.360
Total length (seconds/10 minutes)	127.9±83.6	201.1±120.6	85.8±76.3	117.3±98.7	0.131	0.236

S1= Session 1; S2=Session 2; Exp.=Experimental group; Con.=Control group; *Significantly different ($p<0.05$).

4.2.1 Comparison of Lasting Length

The definition of "lasting length" here is the duration (refer to Fig. 3.12) of an epoch with coupling degree higher than threshold. The histograms of lasting length of nonlinear coupling are presented in Fig. 4.6 for both groups. It shows that most nonlinear coupling epochs emerged from 20 to 40 seconds for both groups of subjects. And there is no apparent difference between groups and between sessions of each group on this distribution. That is, neither inter-group nor intra-group difference was observed. By statistical analysis for the mean values of lasting length of nonlinear

coupling, both groups revealed no significant difference between two sessions in both groups, as shown in Fig. 4.7 and Table 4.2. This indicates that, in general, neither meditation nor rest could noticeably affect the lasting length of nonlinear coupling.

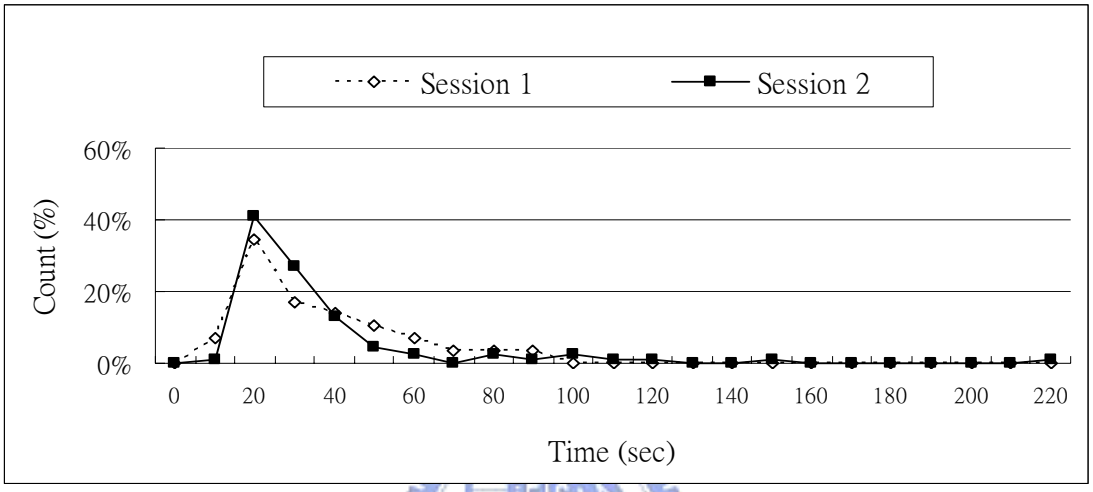

(a)

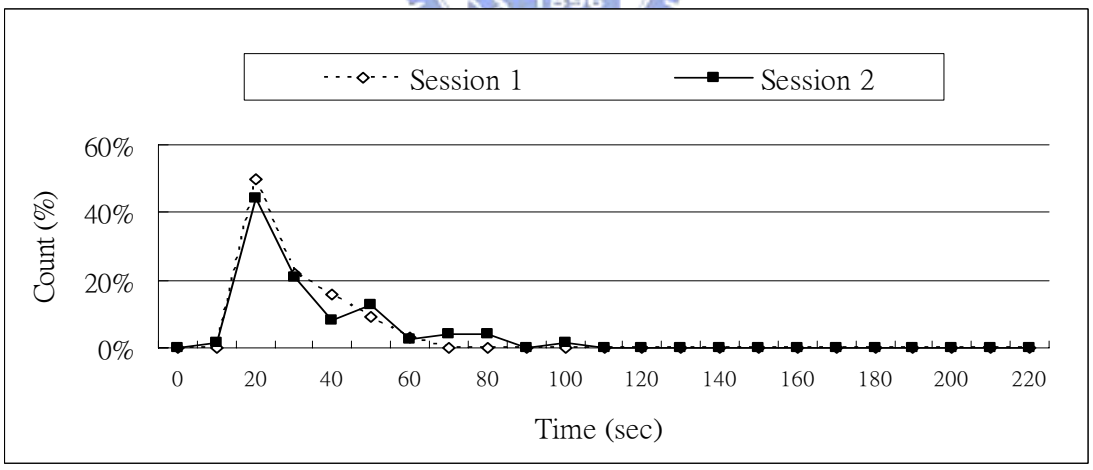

(b)

Fig. 4.6 Histograms of lasting length of nonlinear coupling for (a) experimental group and (b) control group.

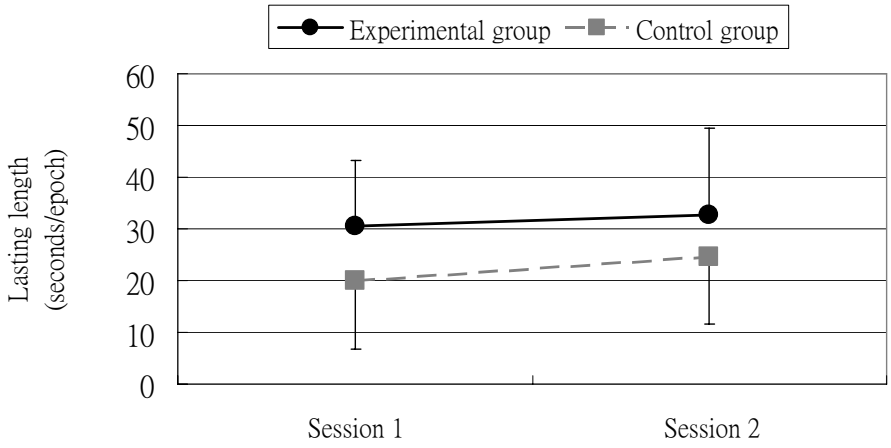

Fig. 4.7 Mean values of lasting length of nonlinear coupling for both groups in different recording sessions.

4.2.2 Comparison of Number of Epochs

The definition of "number of epochs" here is the amount of epochs with coupling degree higher than threshold in a ten minutes time duration. As shown in Fig. 4.8 and Table 4.2, the mean values of the number of nonlinear coupling epochs revealed insignificant difference between main session (Session 2, at rest) and pre-session (Session 1, background recording) in control group. As regards the experimental group, it increased considerably during meditation (Session 2: 6.1±2.5 counts/10 minutes), in comparison with the mean number observed in the pre-session background recording (4.1±2.3 counts/10 minutes).

4.2.3 Comparison of Total Length

The definition of "total length" here is the sum of lengths of all epochs with coupling degree higher than threshold in a 10 minutes time period. As shown in Fig. 4.9 and Table 4.2, the mean values of the total length of nonlinear coupling revealed insignificant difference between main session (Session 2) and pre-session (Session 1, background recording) in both groups.

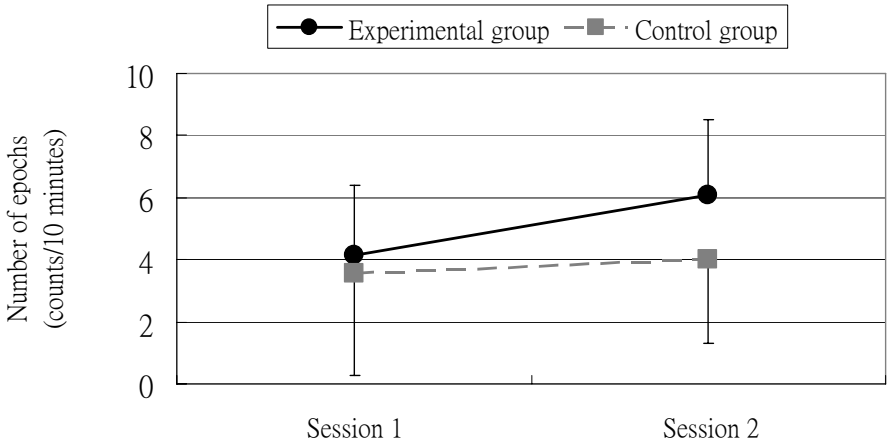

Fig. 4.8 Variations of mean number of nonlinear coupling epochs for both groups in different recording sessions.

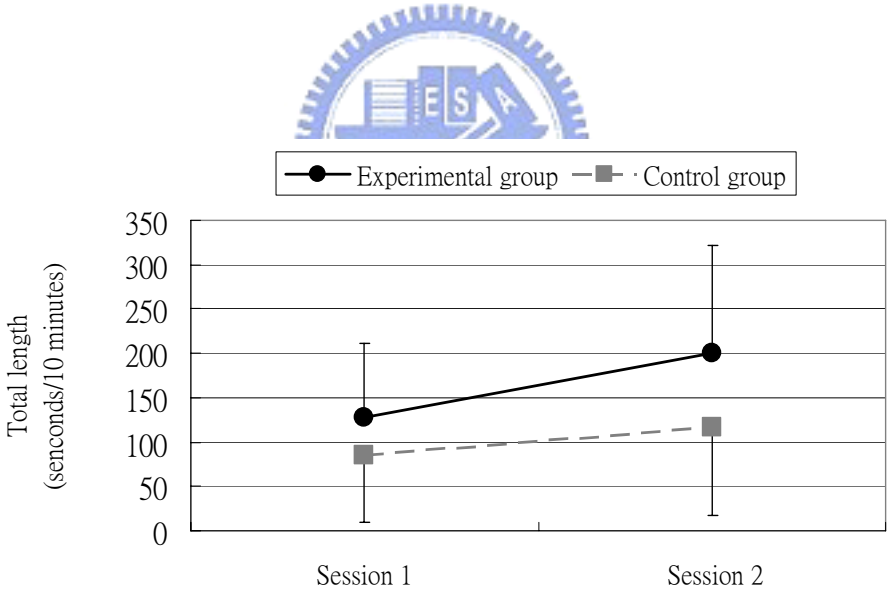

Fig. 4.9 Mean values of total length of nonlinear coupling for both groups in different recording sessions.

4.3 Correlation between Phase Synchronization and Nonlinear Coupling

As introduced in Chapter 1, synchronization is a phenomenon that occurs due to interaction of two or more self-sustained oscillators. Therefore, there must exist some forms of couplings between oscillators to carry out the interaction. Based on this concept, we brought forward the hypothesis that the nonlinear coupling nature of cardiorespiratory system determined by time-phase cross-bispectral analysis could be correlated with cardiorespiratory phase synchronization in a sense.

To examine this hypothesis, we made a qualitative observation on both the instantaneous degree of phase synchronization and the nonlinear coupling. In addition, we conducted a quantitative analysis by calculating the correlation coefficients between them.

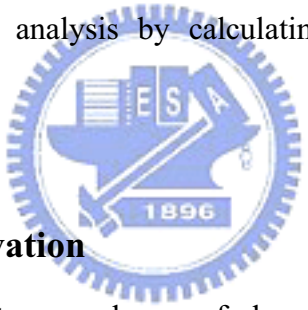

4.3.1 Qualitative Observation

Fig. 4.10 plots the instantaneous degree of phase synchronization and nonlinear coupling for four subjects (two experimental and two control subjects). The instantaneous degree of nonlinear coupling and of phase synchronization is illustrated in red and blue, respectively. According to naked-eye examination on these figures, we found some degree of coincidence existing between these two curves. Some sample events include: (Fig. 4.10 (a)) 0-2 minute of Session 1, (Fig. 4.10 (b)) 0-5 minute of Session 1 and 0-20 minute of Session 2, (Fig. 4.10 (c)) 20-25 minute of Session 2, and (Fig. 4.10 (d)) 7-16 minute of Session 2. These events are identified by gray bars in the figures. Next, we further quantify the coincidence by correlation coefficient analysis in the following section.

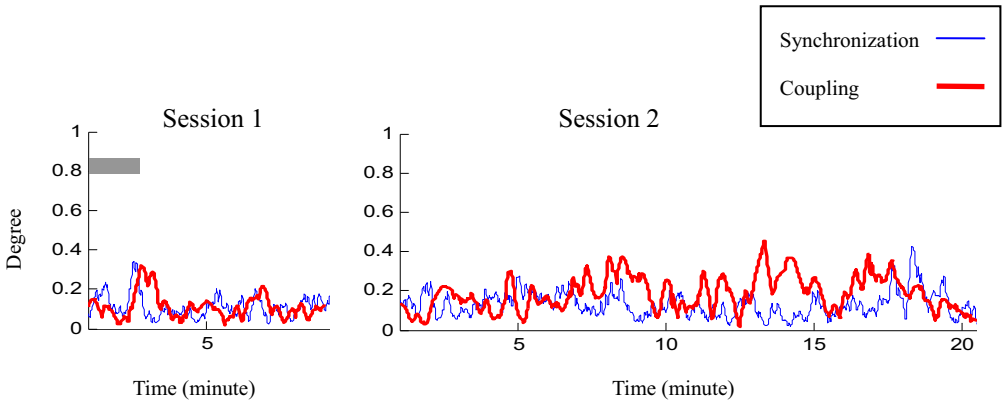

(a)

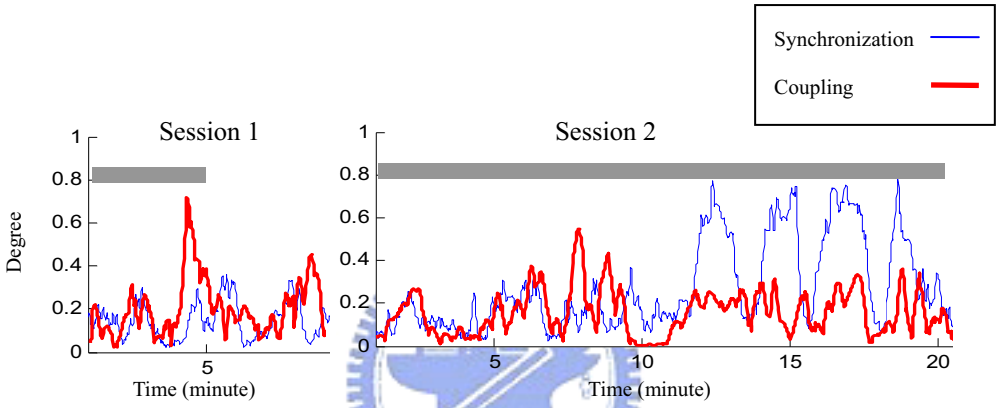

(b)

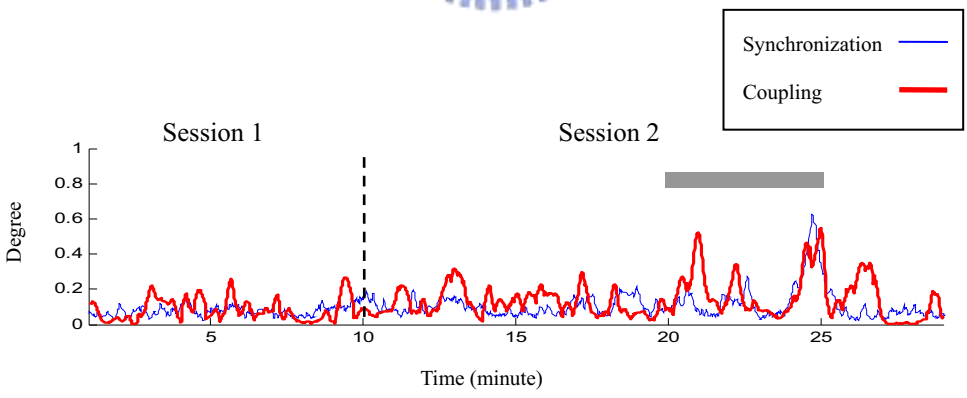

(c)

Fig. 4.10 Instantaneous degree of (blue) the phase synchronization and (red) the nonlinear coupling (subjects : (a) experimental subject 0928, (b) experimental subject 1003, (c) control subject 0411, and (d) control subject 0727).

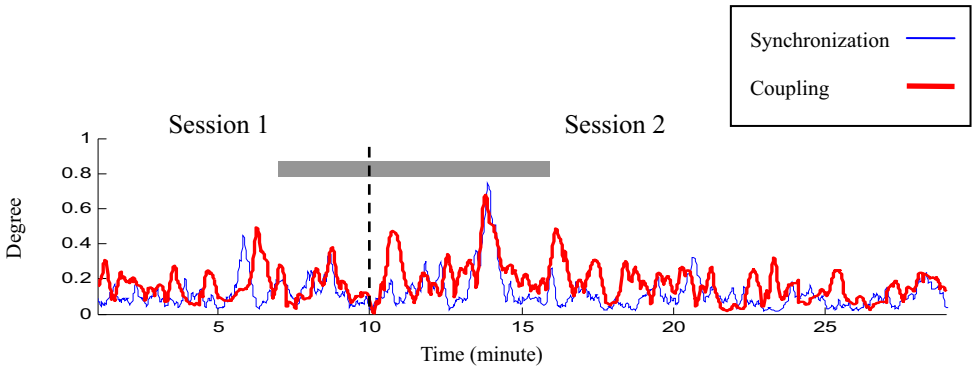

(d)

Fig. 4.10 (Continued).

4.3.2 Quantitative Analysis

To quantify the coincidence between phase synchronization and nonlinear coupling, we first interpolated the sequences (with 1 second resolution) for the instantaneous degree of both the phase synchronization and the nonlinear coupling. Next, the correlation coefficients were calculated for these two new sequences using two-minute window size with one-minute overlap. The results displayed in Fig. 4.11 illustrate the time course of correlation coefficients $\gamma(d)$ for each of the four subjects (two experimental and two control subjects). In general, the range of correlation coefficient is interpreted by: 1) $\gamma(d)<0.3$: low correlation, 2) $0.3\leq\gamma(d)<0.7$: moderate correlation, and 3) $\gamma(d)\geq0.7$: high correlation. Accordingly, we roughly classified the correlation into three states: positive correlation ($\gamma(d)\geq0.3$), negative correlation ($\gamma(d)\leq-0.3$), and little correlation ($-0.3<\gamma(d)<0.3$). In Fig. 4.11, the intervals with correlation coefficients higher than 0.3 (positive correlation) are marked by gray bars on the top of each bar chart. The results closely coincide with those of qualitative examination presented in section 4.3.1.

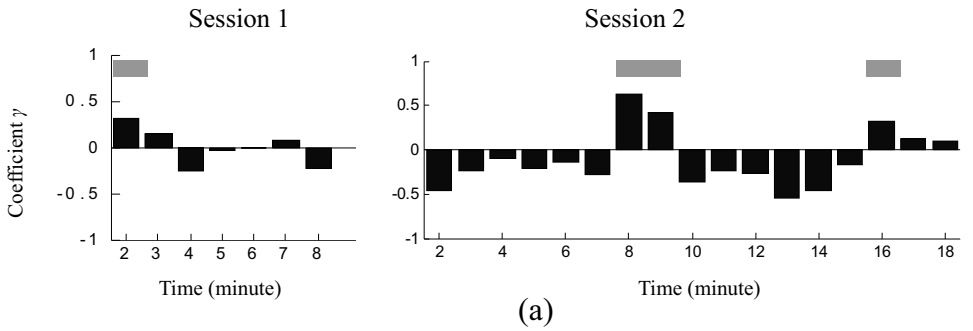

(a)

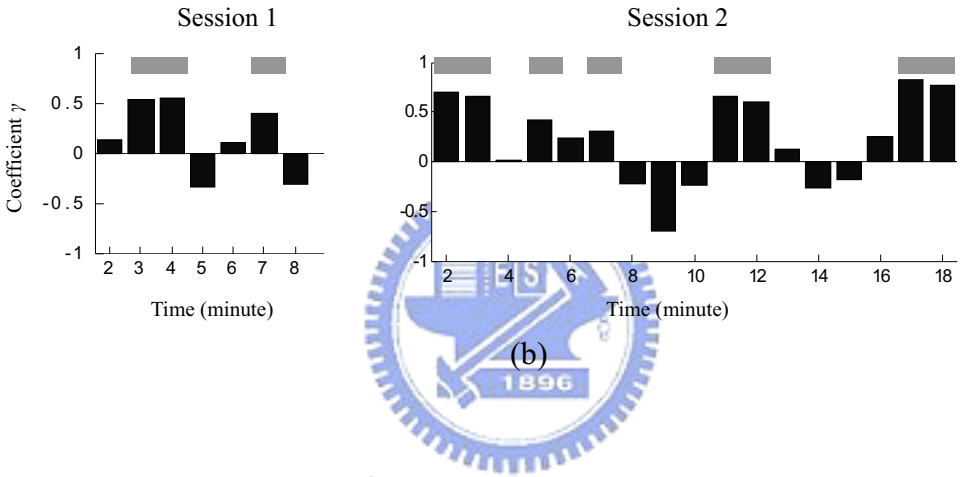

(b)

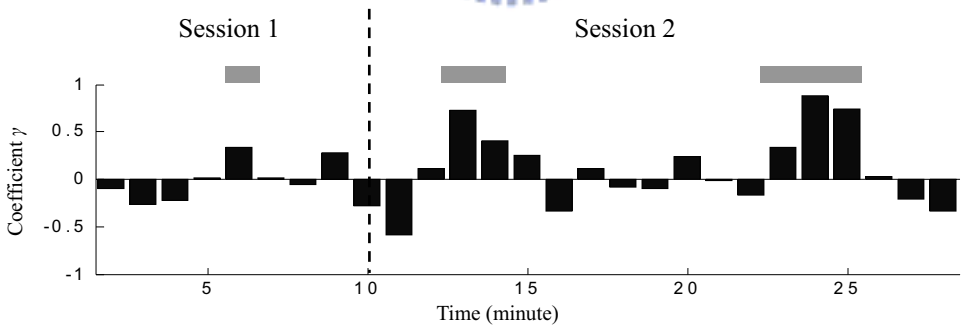

(c)

Fig. 4.11 Time course of correlation coefficient between the phase synchronization and the nonlinear coupling (subjects : (a) experimental subject 0928, (b) experimental subject 1003, (c) control subject 0411, and (d) control subject 0727).

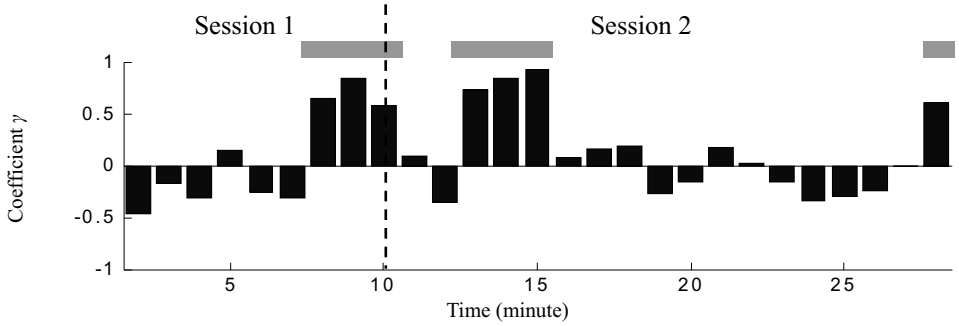

(d)

Fig. 4.11 (Continued).

The histograms of correlation coefficients are presented in Fig. 4.12 for both groups. In the figures, the regions corresponding to three correlation states are separated by thick vertical lines. These figures reveal a higher percentage of positive correlation and a lower percentage of negative correlation derived for the experimental group as compared with the control group, especially during Session 2 (meditation). Table 4.3 lists, for each group in a given session, the percentage of total time interval of each correlation state. To examine the statistical significance of percentage difference between Session 1 and Session 2, the paired *t* test was applied and the significant levels were selected to be $p<0.05$. Apparently, only the percentage of positive correlation increases significantly in experimental group from Session 1 (rest, 28.6%) to Session 2 (meditation, 43.7%). And, for the control group, there is no significant difference between Session 1 and Session 2, considering each particular correlation state.

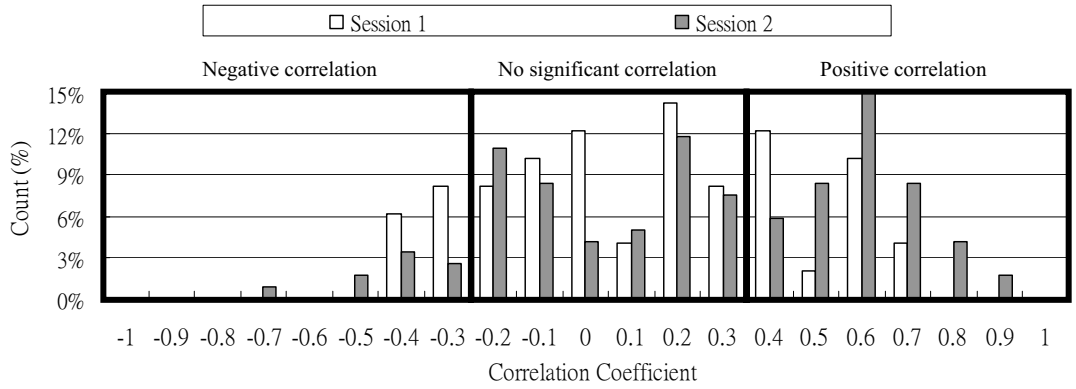

(a)

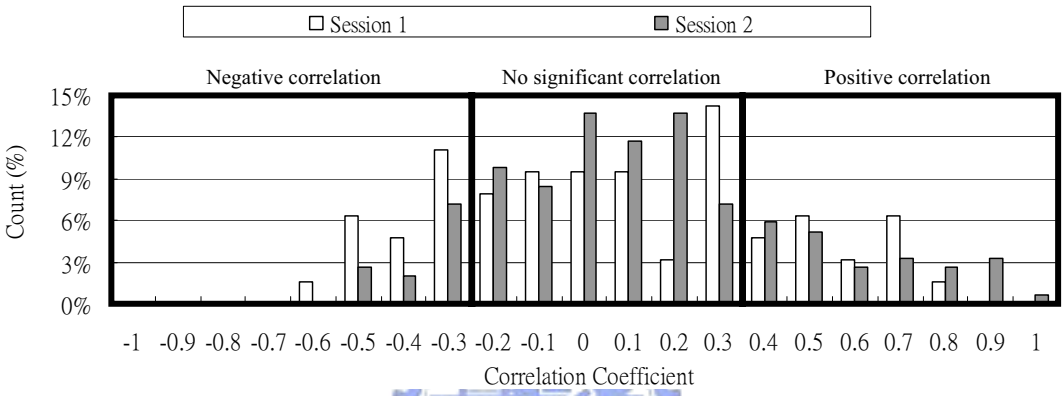

(b)

Fig. 4.12 Histograms of correlation coefficient between the phase synchronization and the nonlinear coupling for (a) experimental group and (b) control group.

Table 4.3 Percentage of total time interval of each correlation state.

Correlation states	Experimental Group (n=7)		Control Group (n=9)		*p*-Value for comparison of	
	S1	S2	S1	S2	Exp. Group S1 vs. S2	Con. Group S1 vs. S2
Positive correlation ($\gamma(d)\geq 0.3$)	28.6%	43.7%	22.2%	23.5%	0.011*	0.451
Negative correlation ($\gamma(d)\leq -0.3$)	14.3%	8.4%	23.8%	11.8%	0.211	0.111
No significant correlation ($-0.3<\gamma(d)<0.3$)	57.1%	47.9%	54.0%	64.7%	0.154	0.094

S1= Session 1; S2=Session 2; Exp.=Experimental group; Con.=Control group; *Significantly different ($p<0.05$).

We further examined tempo of occurrence of two different types of correlation, positive and negative, by measuring the continuous duration of each correlation state. The results are shown in Fig. 4.13. Note that most segments last no longer than two minutes.

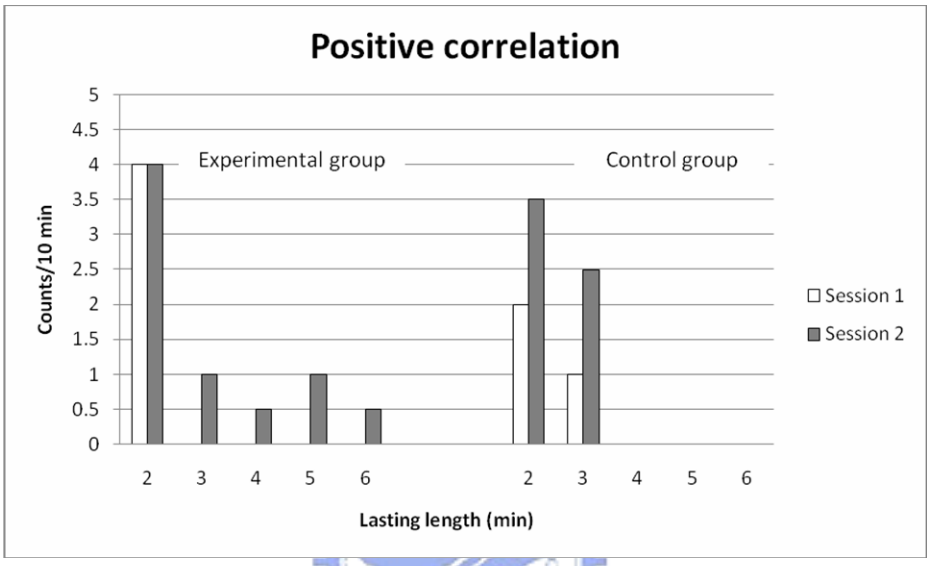

(a)

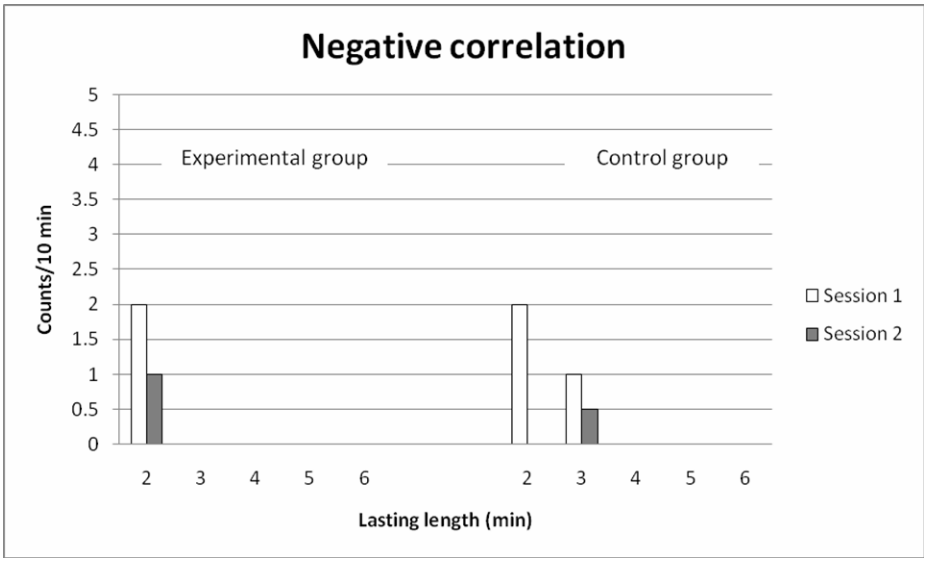

(b)

Fig 4.13 Histograms of lasting length of the segment identified to be (a) the positive, or (b) the negative correlation.

Chapter 5
Conclusion and Discussion

5.1 Conclusion and Discussion

This thesis has reported our study on various synchronous phenomena in the cardiorespiratory system. The main aim of this research was to investigate the effects of Zen meditation on the phenomenon of synchronization and the nature of nonlinear coupling in the cardiorespiratory systems of the experimental (meditating) and control (non-meditating) group.

In regard to the study on synchronization phenomenon, most synchronous epochs appeared in short length (from 10 to 30 seconds) for subjects at rest. This fact reflects that the interaction between cardiac and respiratory systems is weak in normal healthy subjects. Nonetheless, Zen meditation was found to cause effects on synchronization. Number of the synchronous epochs and the total synchronization length increased significantly (p=0.023 and p=0.034, respectively) during meditation as compared with the results for subjects at rest. Of course, hardly identifiable difference was observed between two sessions for the control group. We therefore might infer from the results that meditation produces different effects on cardiorespiratory synchronization other than normal rest does. According to the literature, high degree of synchronization correlates to a possibly high energetic benefit by respiration and heart beating [5], that might reflect good feedback mechanisms or interconnections [28]. We thus assume that meditation could preserve bodily energy and enhance the feedback mechanisms or interconnections between these two systems.

In the aspect of investigating the nature of nonlinear coupling, we also found that most coupling lengths were short (from 20 to 40 seconds), in agreement with the suggestion that nonlinear coupling between respiratory and cardiac rhythms was weak in normal healthy subjects [10]. In our study on meditation practitioners, the effect of meditation on cardiorespiratory coupling was evident. Number of the coupling epochs increased significantly ($p = 0.038$) during meditation as compared with that studied on subjects at rest. As being anticipated, there existed trivial difference of the coupling nature between two sessions in the control group.

In regard to the coincidence between phase synchronization and nonlinear coupling of cardiorespiratory system, three correlation states (positive correlation, negative correlation, and low correlation) were presented for both groups. And the continuous durations of both positive and negative correlation states were measured. We found that most segments lasted no longer than two minutes. According to the results, these two schemes do not coincide on the case of analyzing cardiorespiratory system. There may be other unknown mechanisms modulating the synchronization phenomenon (synchronization or desynchronization) and the nonlinear coupling may play the role of investigating the cardiorespiratory interactions. Further, we found that the percentage of positive correlation increased significantly ($p = 0.011$) during meditation. Moreover, the positive correlation could last longer. It suggests that under nonlinear coupling, meditation might enhance the phase synchronization between cardiac and respiratory systems.

5.2 Future Work

In this study, we only investigated the coupling nature of characteristic frequencies of ECG and respiratory signals. The coupling caused by interaction of some other frequency components may play an important role in studying the physiological model under meditation. Besides, it has been reported in the literatures that cardiorespiratory synchronization might be related to the central neural regulation [3] and brain activity [8]. Hence, for profound understanding of the Zen-meditation process and effects, EEG signals should be included to explore the mutual interaction between the brain and cardiorespiratory system. For example, analysis of heart rate variability could reflect the influence of autonomic nervous system.

References

[1] Berntson G.G., Cacioppo J.T., Quigley K.S., "Respiratory sinus arrhythmia: autonomic origins, physiological mechanisms, and psychophysiological implications," *Psychophysiology*, vol.30(2), pp.183－196, March 1993.

[2] Giardino N.D., Glenny R.W., Borson S., Chan L., "Respiratory sinus arrhythmia is associated with efficiency of pulmonary gas exchange in healthy humans," *Am. J. Physiol. Heart Circ. Physiol.*, vol.284(5), pp.H1585－H1591, 2003.

[3] Schäfer C., Rosenblum M. G., Abel H.-H., Kurths J., "Synchronization in the human cardiorespiratory system," *Phys. Rev. E*, vol.60(1), pp.857－870, July 1999.

[4] Schäfer C., Rosenblum M. G., Kurths J., Abel H.-H., "Heartbeat synchronised with respiration," *Nature*, vol.392(6673), pp.239－241, Mar. 1998.

[5] Toledo E., Akselrod S., Pinhas I., Aravot D., "Does synchronization reflect a true interaction in the cardiorespiratory system?," *Med Eng Phys*, vol.24(1), pp.45－52, Jan. 2002.

[6] Lotric M.B., Stefanovska A., "Synchronization and modulation in the human cardiorespiratory system," *Physica A: Statistical Mechanics and its Applications*, vol.283(3-4), pp.451－461, Aug. 2000.

[7] Stefanovska A., Lotric M.B., Strle S., Haken H., "The cardiovascular system as coupled oscillators? ," *Physiol. Meas.*, vol.22(3), pp.535－550, March 2001.

[8] Bartsch R., Kantelhardt J. W., Penzel T., Havlin S., "Experimental evidence for phase synchronization transitions in the human cardiorespiratory system," *Phys. Rev. Lett*, vol.98(5), Feb. 2007.

[9] Stefanovska A., Haken H., McClintock P.V.E., Hozic M., Bajrovic F., Ribaric S., "Reversible transitions between synchronization states of the cardiorespiratory system," *Phys. Rev. Lett.*, vol.85(22), pp.4831－4834, Nov. 2000.

[10] Jamšek J., Stefanovska A., McClintock P. V. E., "Nonlinear cardio-respiratory interactions revealed by time-phase bispectral analysis," *Phys. Med. Biol.*, vol.49(18), pp:4407－4425, Sep. 2004.

[11] Blekhman I.I., *Synchronization in Science and Technology*. New York: American Society of Mechanical Engineers, Sep. 1988.

[12] Rosenblum M. G., Pikovsky A. S., Kurths J., "Phase synchronization of chaotic oscillators," *Phys. Rev. Lett.*, vol.76(11), pp.1804－1807, March 1996.

[13] Nikias C.L., Petropulu A.P., *Higher-Order Spectra Analysis: A Nonlinear Signal Processing Framework.* Englewood Cliffs, N.J.: Prentice-Hall, 1993.

[14] Jamšek J., Stefanovska A., McClintock P. V. E., Khovanov I. A., "Time-phase bispectral analysis," *Phys. Rev. E*, vol.68(1), July 2003.

[15] Peng C.K. , Mietus J. E., Liu Y., Khalsa G., Douglas P. S., Benson H., Goldberger A.L., "Exaggerated heart rate oscillations during two meditation techniques," *International Journal of Cardiology*, vol.70(2), pp.101－107, 1999.

[16] Peng C.K., Henry I.C., Mietus J.E., Hausdorff J.M., Khalsa G., Benson H., Goldberger A.L., "Heart rate dynamics during three forms of meditation," *International Journal of Cardiology*, vol.95(1), pp.19－27, May 2004.

[17] Cysarz D., Büssing A., "Cardiorespiratory synchronization during Zen meditation," *European Journal of Applied Physiology*, vol.95(1), pp.88－95, Sep. 2005.

[18] 陳德輝, *心電圖學原理與實用.* 初版, 臺北市: 合記圖書出版社, 1972.

[19] Carr J.J., Brown J.M., *Introduction to Biomedical Equipment Technology.* 4th ed, Upper Saddle River, N.J.: Prentice Hall, May 2000.

[20] Crouch J.E., McClintic J.R., *Human Anatomy and Physiology.* 2nd ed, New York: Wiley, 1976.

[21] Stefanovska A., Bracic M., "Physics of the human cardiovascular system," *Contemp. Phys.*, vol.40(1), pp.31－55, 1999.

[22] Stratonovich R.L., *Topics in the Theory of Random Noise.* New York: Gordon and Breach, 1963.

[23] Pikovsky A., Rosenblum M., Kurths J., "Phase synchronization in regular and chaotic systems," *International Journal of Bifurcation and Chaos*, vol.10(10), pp. 2291－2305, 2000.

[24] Rosenblum M.G., Pikovsky A.S., Kurths J., Schäfer C., Tass P.A., "Phase synchronization: from theory to data analysis," *in Neuro-informatics and Neural Modeling, volume 4 of Handbook of Biological Physics.* eds. Moss F. and Gielen S., Amsterdam: Elsevier Science, 2001.

[25] Goldshlager N., Goldman M.J., *臨床心電圖學.* 廖述朗, 初版, 臺北市: 藝軒圖書出版社, 1995.

[26] Kadambe S., Murray R., Boudreaux-Bartels G.F., "Wavelet transform-based QRS complex detector," *IEEE transactions on bio-medical engineering*, vol.46(7), pp.838－848, July 1999.

[27] Köhler B.U., Hennig C., Orglmeister R., "The principles of software QRS detection," *IEEE engineering in medicine and biology magazine*, vol.21(1), pp.42－57, January 2002.

[28] Mrowka R., Patzak A., Rosenblum M.G., "Quantitative analysis of cardiorespiratory synchronization in infants," *International journal of bifurcation and chaos in applied sciences and engineering*, vol.10(11), pp.2479－2488, 2000.

Appendix A
Detection of ECG R Peak and Respiratory Peak

A.1 R-Peak Detection

The flow chart of R peak detection is shown in Fig. A.1.

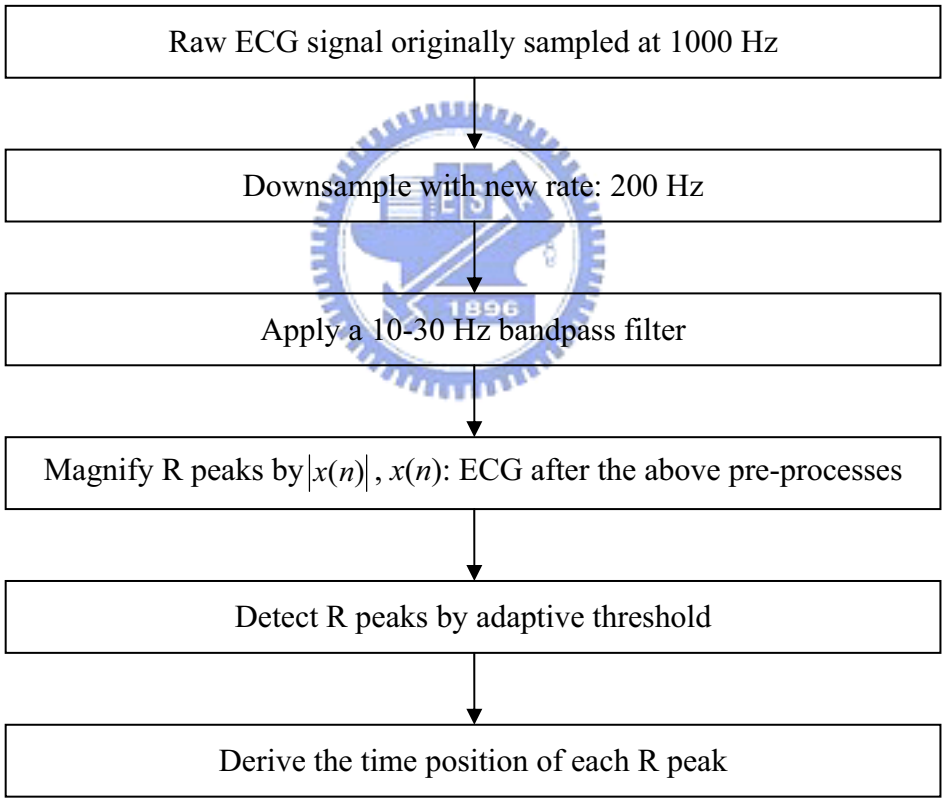

Fig. A.1 Flow chart of R peak detection.

Step 1. Downsampling of Raw ECG Signal

Raw ECG signal originally recoded at 1000Hz (required by the other researches) was firstly downsampled with new sampling rate of 200 Hz, utilizing Matlab's

built-in polyphase filter implementation, including an anti-aliasing (lowpass) FIR filter.

Step 2. Noise Reduction by Bandpass Filtering

ECG signal after downsampling was then filtered by a 10-30 Hz bandpass filter to reduce the baseline drift and high frequency noise (e.g. 60Hz power line noise, EMG signal) and further enhance the R peaks.

Step 3. Magnification of R Peaks

R peaks were magnified by multiplying ECG signal $x(n)$ by its absolute-valued signal $|x(n)|$ to generate an R-magnified signal $x'(n) = x(n) \times |x(n)|$. As shown in Fig. A.2, the ECG signal before and after preprocessing is presented. Note that the amplitudes of R peaks are obviously enhanced and cleansed.

Step 4. R-Peak Detection by Adaptive Threshold

The threshold for R peak detection was determined for every one-minute frame, that was selected to be 0.3 time of the maximum ECG amplitude within the frame. Adaptive-threshold scheme was adopted for the reason that the range of ECG amplitude varies among subjects. Moreover, inter-subject variations are often inevitable in biomedical signals.

Step 5. Acquisition of R-Peak Locations in Time

For each QRS complex, there will exhibit a time duration that its amplitude bigger than the threshold as shown in Fig. A.3. The maximum amplitude during this time duration was determined, and its time position was employed as the time position of R peak.

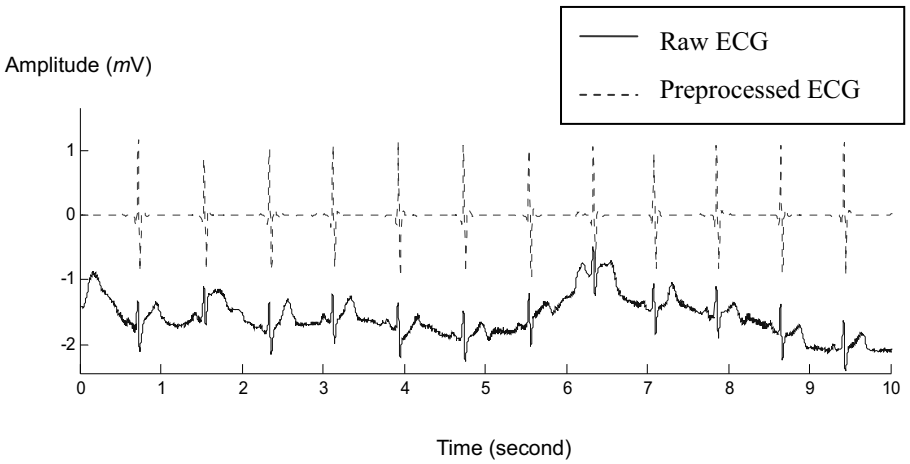

Fig. A.2 The raw ECG and preprocessed ECG.

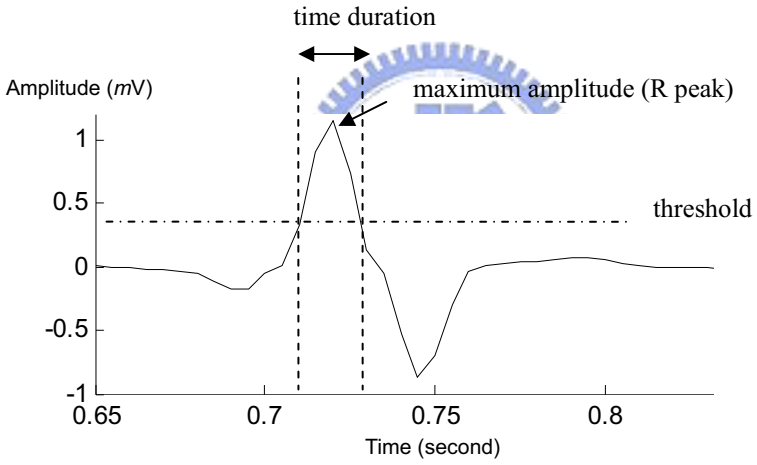

Fig. A.3 R peak detection by threshold.

A.2 Respiratory Peak Detection

The flow chart of Respiratory peak detection is shown in Fig. A.4.

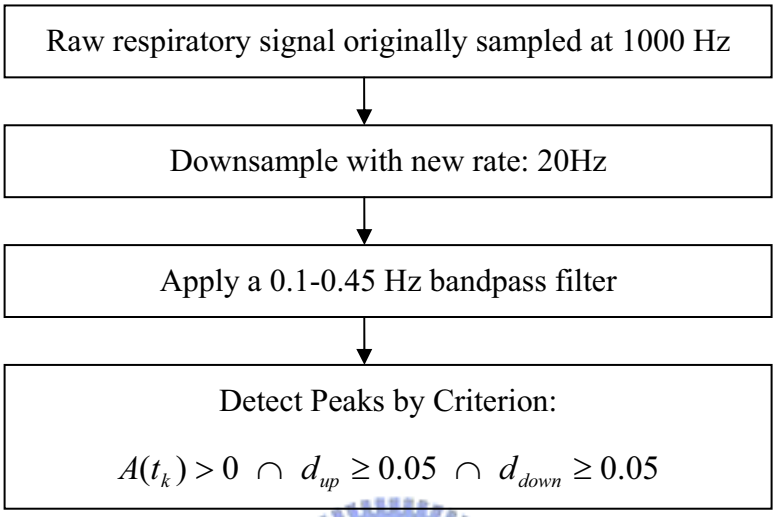

Fig. A.4 Flow chart of Respiratory peak detection.

Step 1. Downsampling of Raw Respiratory Signal

The raw respiratory signal originally recorded at 1000 Hz (required by the other researches) was firstly downsampled with new sampling rate of 20 Hz, utilizing Matlab's built-in polyphase filter implementation, including an anti-aliasing (lowpass) FIR filter.

Step 2. Noise Reduction by a Bandpass Filtering

Respiratory signal after downsampling was then filtered by a 0.1-0.45 Hz bandpass filter to reduce the baseline drift and make the wave smoother. The respiratory signal before and after preprocessing is shown in Fig. A.5.

Step 3. Detect Peaks of Respiratory Signal

The filtered respiratory signal was then normalized by its maximum value of

positive amplitude and the local maxima of its amplitude were derived. At last, these local maxima were considered as peaks by the following criterion:

$$A(t_k) > 0 \ \cap \ d_{up} \geq 0.05 \ \cap \ d_{down} \geq 0.05 \qquad \text{(A.1)}$$

where t_k is the time position of k_{th} respiratory peak and $A(t_k)$ is its amplitude; d_{up} is the amplitude of inspiration and d_{down} is the amplitude of expiration. These parameters are illustrated in Fig. A.6.

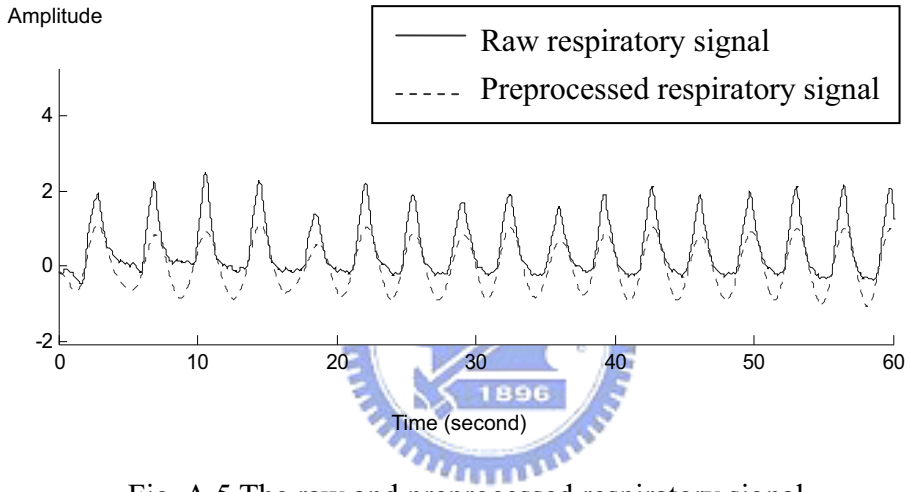

Fig. A.5 The raw and preprocessed respiratory signal.

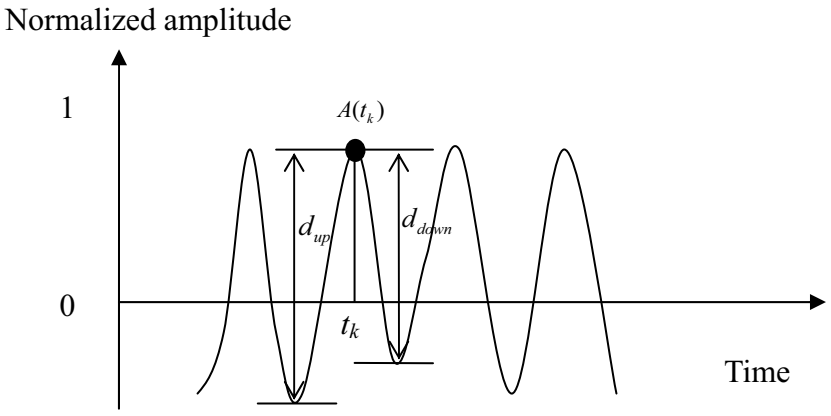

Fig. A.6 Parameters for respiratory signal peak detection.